Modified Windmill Porphyrin Arrays: Coupled Light-Harvesting and Charge Separation, Conformational Relaxation in the S_1 State, and $S_2 - S_2$ Energy Transfer

Aiko Nakano,[a] Atsuhiro Osuka,*[a] Tomoko Yamazaki,[b] Yoshinobu Nishimura,[b] Seiji Akimoto,[b] Iwao Yamazaki,*[b] Akira Itaya,[c] Masataka Murakami,[c] and Hiroshi Miyasaka*[c]

Abstract: The architecture of windmill hexameric zinc(II)–porphyrin array **1** is attractive as a light-harvesting functional unit in view of its three-dimensionally extended geometry that is favorable for a large cross-section of incident light as well as for a suitable energy gradient from the peripheral porphyrins to the *meso*–*meso*-linked diporphyrin core. Three core-modified windmill porphyrin arrays **2**–**4** were prepared for the purpose of enhancing the intramolecular energy-transfer rate and coupling these arrays with a charge-separation functional unit. Bisphenylethynylation at the *meso* and *meso'* positions of the diporphyrin core indeed resulted in a remarkable enhancement in the intramolecular $S_1 - S_1$ energy transfer in **2** with $\tau = 2 \sim 3$ ps, as revealed by femtosecond time-resolved transient absorption spectroscopy. The fluorescence lifetime of the S_2 state of the peripheral porphyrin energy donor determined by the fluorescence up-conversion method was 68 fs, and thus considerably shorter than that of the reference monomer (150 fs), suggesting the presence of the intramolecular energy-transfer channel in the S_2 state manifold. Such a rapid energy transfer can be understood in terms of large Coulombic interactions associated with the strong Soret transitions of the donor and acceptor. Picosecond time-resolved fluorescence spectra and transient absorption spectra revealed conformational relaxation of the S_1 state of the diporphyrin core with $\tau = 25$ ps. Upon photoexcitation of models **3** and **4**, which bear a naphthalenetetracarboxylic diimide or a *meso*-nitrated free-base porphyrin attached to the modified diporphyrin core as an electron acceptor, a series of photochemical processes proceeded, such as the collection of the excitation energy at the diporphyrin core, the electron transfer from the S_1 state of the diporphyrin to the electron acceptor, and the electron transfer from the peripheral porphyrins to the diporphyrin cation radical, which are coupled to provide a fully charge-separated state such as that in the natural photosynthetic reaction center. The overall quantum yield for the full charge separation is better in **4** than in **3** owing to the slower charge recombination associated with smaller reorganization energy of the porphyrin acceptor.

Keywords: molecular devices · photochemistry · porphyinoids · photosynthesis · supramolecular chemistry

Introduction

There are two major functional components, namely the light-harvesting (antenna) complex (LHC) and the reaction center (RC), in photosynthetic reaction centers, which are responsible for the energy source of all the living things. The LHC has role of broadening the cross section and spectral region of the incident light and of delivering the captured excitation energy to the RC without any serious energy loss.[1] The RC in turn has a quantitative charge-separation function to convert light energy to chemical potential that fuels cellular processes.[2] Effective coupling of these two major functions, which is vital for photosynthesis, is attained by a protein matrix that holds chromophores and electron carriers at the precise distances and in the correct orientations.

In view of the importance of photosynthesis, many model systems have been prepared in which porphyrins are covalently joined by a variety of bridges,[3–5] although there have been only scattered examples of models in which the two major functions of light-harvesting and charge separation are effectively coupled in a single molecule to produce a long-lived charge-separated state for photoexcitation in a wide wavelength range.[6]

[a] Prof. A. Osuka, A. Nakano
Department of Chemistry, Graduate School of Science
Kyoto University, Kyoto 606-8502 (Japan)
Core Research for Evolutional Science and Technology (CREST) of Japan Science and Technology Corporation (JST) (Japan)
Fax: (+81) 75-753-3970
E-mail: osuka@kuchem.kyoto-u.ac.jp

[b] Prof. I. Yamazaki, Dr. T. Yamazaki, Dr. Y. Nishimura, Dr. S. Akimoto
Department of Chemical Process Engineering
Graduate School of Engineering
Hokkaido University, Sapporo 060-8628 (Japan)

[c] Prof. H. Miyasaka, Prof. A. Itaya, M. Murakami
Department of Polymer Science and Engineering
Kyoto Institute of Technology, Kyoto 606-8585 (Japan)

© WILEY-VCH Verlag GmbH, D-69451 Weinheim, 2001
0947-6539/01/0714-3134 $ 17.50+.50/0

Recently, we developed an efficient synthetic route to windmill porphyrin arrays that have three-dimensionally arranged orthogonal geometry, which is favorable for the large cross section of the incident light.[7] The direct *meso*–*meso* connection in the diporphyrin core results in the stabilization of the S_1 state and thus enables an efficient energy transfer from the peripheral porphyrins to the diporphyrin core. The efficiency of the energy transfer process has been estimated to be about 96%, but the observed double exponential fluorescence decay profile of the peripheral porphyrins suggested the presence of a reverse energy-transfer process due to a small energy difference between the S_1 states of the donor and acceptor.[7]

An advantageous feature of the artificial models lies in their flexible tunability in response to required functional demands. Herein we describe attempts to improve the efficiency of the intramolecular energy transfer from the peripheral porphyrins to the diporphyrin core by chemical modification. Taking advantage of the free *meso* positions of the windmill porphyrin arrays, we attempted the phenylethynylation at the *meso* positions with the expectation that the energy level of the S_1 state of the diporphyrin core can be lowered with respect to that of the peripheral porphyrins, thereby enhancing the energy transfer from the peripheral porphyrins.[8] This molecular design was triggered by recent reports that *meso*-ethynylation and *meso*-butadiynylation of porphyrins led to substantial decreases in the S_1 state energy level. Arnold et al. reported the red-shifted absorption band of butadiyne-bridged nickel(II) diporphyrin[9] and Therien et al. showed that the excitation energy of the S_1 state of zinc(II) 5,15-diphenyl-10-trimethylsilylethynylporphyrin is about 2.04 eV; that is, considerably lower than that of the parent zinc(II) 5,15-diphenylporphyrin (2.12 eV).[10] Similar spectral changes were also reported independently by Anderson and co-workers[11] and Milgrom and co-workers.[12] *meso*-Ethynylated and -butadiynylated zinc(II) porphyrins have attracted considerable interest mainly due to their fascinating optical properties, but little attention has been paid to their use as an energy-accepting functional unit towards the normal zinc(II) porphyrins.[8a]

Herein, we also report the extension of this strategy to more elaborate photosynthetic models in which the energy transfer is designed to be coupled to the subsequent consecutive electron-transfer steps, finally providing a long-lived fully charge-separated state in a single molecule.

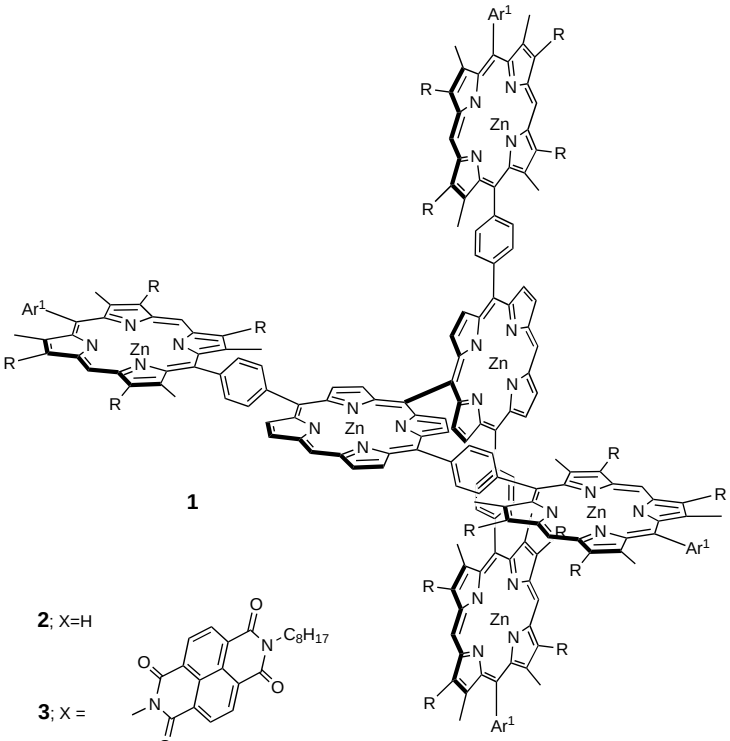

2; X=H

3; X =

4; X =

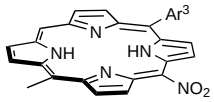

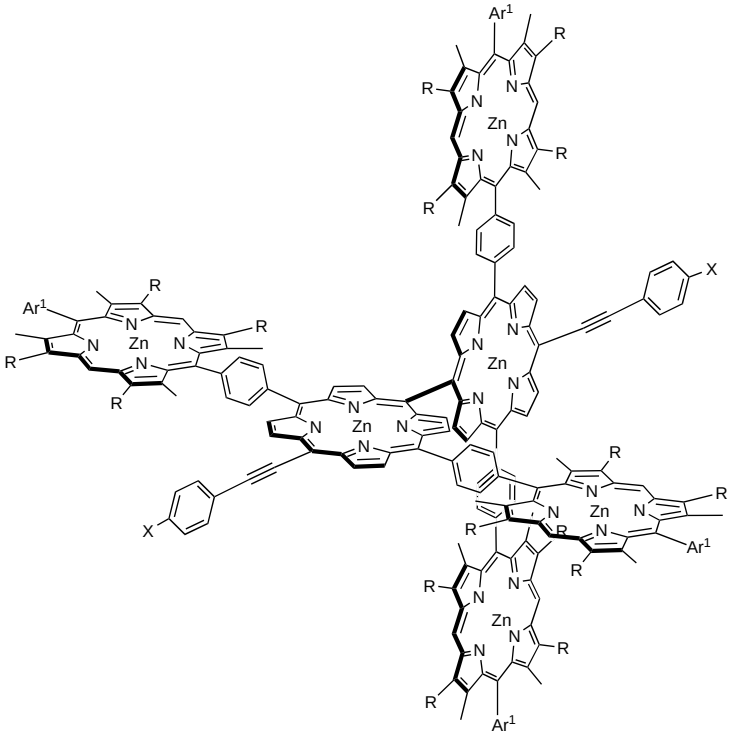

Results

Molecular design: An advantageous feature of the windmill porphyrin hexamer **1** ($Ar^1 = 3,5$-di-octyloxyphenyl, $R = C_6H_{13}$) as a light-harvesting functional unit is the favorable energy gradient from the peripheral porphyrin to the *meso*–*meso*-linked diporphyrin in the S_1 state. Namely, the S_1 state of the peripheral porphyrin has the excitation energy of 2.13 eV, while the S_1 state of the diporphyrin core has the excitation energy of 2.07 eV.[7, 13] The energy difference (0.06 eV) enables the excitation energy flow from the peripheral porphyrin (P) to the diporphyrin core.[7] To improve the efficiency of the energy transfer, we designed model **2** ($Ar^1 = 3,5$-di-octyloxyphenyl, $R = C_6H_{13}$) by bisphenylethynylation at the *meso* and *meso*′ positions of the diporphyrin core with an expectation that the energy level of the S_1 state of the modified diporphyrin core (D) would be sufficiently lowered with

respect to that of the peripheral porphyrin (P) energy donor.[9] Another major aim of the present study is to construct a photosynthetic model, which can perform both light-harvesting and charge separation in a single molecule. With these ideas in mind, we prepared models **3** and **4** (Ar^1 = 3,5-di-octyloxyphenyl, Ar^3 = 2,3,4,5,6-pentafluorophenyl, R = C_6H_{13}), in which two electron acceptors, 1,4,5,8-naphthalene-tetracarboxydiimide (NI)[14, 19b, 25] or *meso*-nitrated free-base porphyrin (F),[15] are attached at the *meso* position of the hexameric windmill porphyrin array through a phenylethynyl spacer. As discussed later, sequential processes have been indeed realized in the models **3** and **4** as follows; the excitation of any P in the array is followed by singlet–singlet energy transfer to D, and the resulting excited state $^1D^*$ donates an electron to the electron acceptor to generate an energetic charge-separated state, P-D^+-NI^- or P-D^+-F^- which evolves to a secondary charge-separated state, P^+-D-NI^- or P^+-D-F^-, by way of hole transfer from the diporphyrin core to the peripheral porphyrin monomer. We also prepared reference compounds **5**–**8** (Ar^2 = 3,5-di-*tert*-butylphenyl, Ar^3 = 2,3,4,5,6-pentafluorophenyl) and **9**–**11** and **20**–**23** (Ar^1 = 3,5-di-octyloxyphenyl, Ar^2 = 3,5-di-*tert*-butylphenyl, Ar^3 = 2,3,4,5,6-pentafluorophenyl) that were necessary to delineate the photoexcited state dynamics of **1**–**4**.

In addition to the light-harvesting and charge separation, we found the conformational relaxation in the S_1 state of *meso*,*meso*′-bisphenylethynylated *meso*–*meso*-linked diporphyrin **6** (D) and also in the D moiety in **2**. Moreover, we found that the S_2 state lifetime of P in **2** was considerably shorter than that of the reference porphyrin, which suggested the energy transfer in the S_2 state manifold.[8b]

Synthesis

The synthetic procedures for the reference compounds **5**–**8** are shown in Scheme 1. *meso*,*meso*′-Bisphenylethynylation of the *meso*–*meso*-linked diporphyrin **5** was carried out essentially by using the procedure developed by Therien et al.[16] Thus, bromination of **5** with *N*-bromosuccinimide (NBS) gave *meso*,*meso*′-dibromoporphyrin **12** in 79% yield, which was transformed into **6** by a Pd-catalyzed Sonogashira coupling reaction[17] with phenylacetylene in 70% yield. The ^{1}H NMR spectrum of **6** showed signals for the four β protons at δ = 9.95, 9.11, 8.66, and 8.11. The signal (H^a) for one pair of the outer β protons adjacent to the phenylethynyl group was downfield shifted by 0.46 ppm relative to that of **5**, probably reflecting the diamagnetic anisotropy current effect of the phenylethynyl substituent at the *meso* position. However, the other three pairs for the β protons were observed at essentially the similar chemical shifts with those of **5**, indicating the similar orthogonal conformation of the diporphyrin core in **6**. Pd-catalyzed coupling reaction of **12** with 4-aminophenylacetylene[18] followed by condensation with **14**[19] gave **7** in 41% yield in two steps. In the preparation of **8**, precursor free-base porphyrin **11** was prepared from 5-(4-trimethylsilylethynylphenyl)-15-pentafluorophenylporphyrin (**15**) in four steps; zinc metalation with $Zn(OAc)_2$, nitration at the *meso* position ($AgNO_2$, I_2),[7b] deprotection of trimethylsilyl group with tetrabutylammonium fluoride (TBAF), and demetalation with HCl.[14] The coupling reaction between **11** and **12** gave **8** in 25% yield.

Scheme 2 summarizes the synthetic routes to the models **2**, **3**, and **4**. In the synthesis of **2**,

© WILEY-VCH Verlag GmbH, D-69451 Weinheim, 2001
0947-6539/01/0714-3136 $ 17.50+.50/0 *Chem. Eur. J.* **2001**, *7*, No. 14

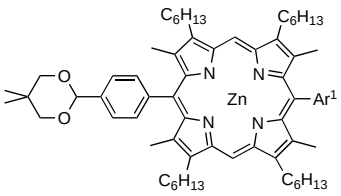

9

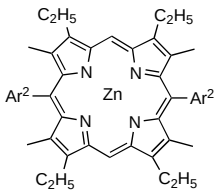

10

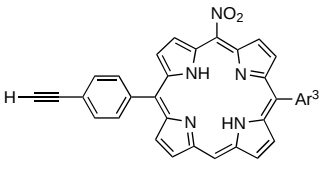

11

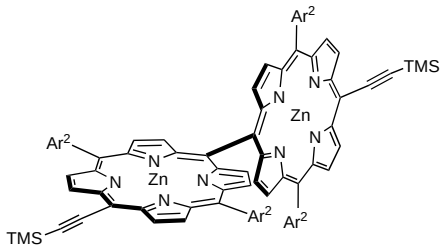

20

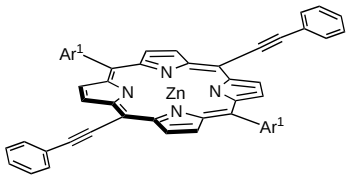

22

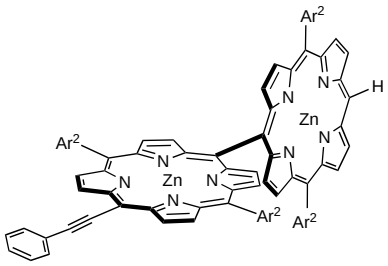

21

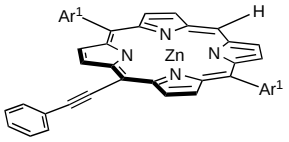

23

we first attempted the bromination of **1** with NBS, which, however, led to extensive decomposition. The electron-rich peripheral zinc(II) β-octaalkylporphyrins were unstable under these bromination conditions and thus we changed a bromination substrate to **16** which bears the peripheral copper(II) β-octaalkylporphyrin in place of zinc(II) β-octaalkylporphyrin. Bromination of **16** with NBS gave dibromide **17**, which was converted into the all-zinc(II)-metalated windmill array **18** by demetalation and remetalation with $Zn(OAc)_2$ with an overall yield of 95% from **16**. Subsequent Pd-catalyzed Sonogashira coupling reaction of **18** with phenylacetylene gave **2** in 33% yield. The Pd-catalyzed coupling reaction of **18** with 4-aminophenylacetylene followed by condensation with **14** gave **3**, and the coupling reaction of **18** with **11** gave **4** in 23% yield. Since the purification of **3** and **4** was very difficult over a silica gel column, their final purification was performed by using recycling preparative GPC–HPLC. Models **3** and **4** exhibited the parent peaks at *m*/*z* 6394 (calcd for $C_{404}H_{494}N_{28}O_{16}Zn_6$, 6391) and *m*/*z* 6675 (calcd for $C_{412}H_{474}F_{10}N_{34}O_{12}Zn_6$, 6677), respectively, in line with their structures.

Reference molecules **20**, **21**, **22**, and **23** were prepared by Pd-catalyzed coupling reaction of *meso*-brominated porphyrins with appropriate acetylenes. [8a]

Absorption and fluorescence spectra

Figure 1 shows the absorption and fluorescence spectra of **5** and **6** recorded in THF. As reported previously, the *meso*–*meso*-linked diporphyrin **5** showed a broad split Soret band at 417 and 452 nm,[7, 13] while the *meso*,*meso*′-bisphenylethynylated diporphyrin **6** exhibited a red-shifted split Soret band at 440 and 474 nm and red-shifted Q bands at 583 and 635 nm. As reported previously,[10] bis-phenylethynylation at 5- and 15-positions donates a large effect to the porphyrin π-conjugated electronic system with their full conjugation, resulting in the removal of the degeneracy of the porphyrin e_g LUMO. This affects the *x*- and *y*-polarized transitions inequivalently and intensifies the quasi-allowed Q band by intensity-borrowing from the Soret transitions.[20] In fact, the Soret band of **22** (not shown) in THF at room temperature was broader (fwhm = 735 cm^{-1}) than those of zinc(II) TPP (TPP = tetraphenylporphyrin; fwhm = 465 cm^{-1}) and zinc(II) 5,15-diarylporphyrin (fwhm = 580 cm^{-1}) and became a clearly split band at 453 and 461 nm at 77 K in 2-methyltetrahydrofuran (MTHF) matrix.[8b] The absorption spectrum of zinc(II) 5-phenylethynylated porphyrin **23** (Figure 2a), which can be regarded as a half-component of **6**, showed only modest influences of single *meso*-phenylethynylation on the electronic properties of the porphyrin, in that the Soret band was observed at 436 nm, the Q bands retained a two-band shape at 566 and 611 nm, and the fluorescence emission was observed with the vibrational bands at 614 and 669 nm. The Soret band of **6**, however, was broader (fwhm = 790 cm^{-1}), indicating some additional perturbation of the porphyrin electronic orbitals by the phenylethynyl substituent.

The absorption spectra of *meso*-phenylethynylated *meso*–*meso*-linked diporphyrin **21** and *meso*,*meso*′-bis(trimethylsilyl)ethynylated *meso*–*meso*-linked diporphyrin **20** are shown in Figures 2b and 2c, respectively. The absorption and fluorescence spectra of **20** were similar to those of **6**, while the absorption spectrum of **21** exhibited a rather broader split Soret band at the high energy side and three distinct Q bands, and the fluorescence spectrum indicated the vibrational mode.

The absorption spectra of **2** and its reference molecules, **6** and **9**, are shown in Figure 3a. A simple absorbance sum of **6** and **9** in a ratio of 1:4 is also shown for comparison. The absorption spectrum of **2** was almost described as a sum of **6** and **9** (1:4) in the Q band region, but considerably broader in the Soret band region. Interestingly, from the analysis of the absorption spectra, we can selectively excite the P moiety in **2**

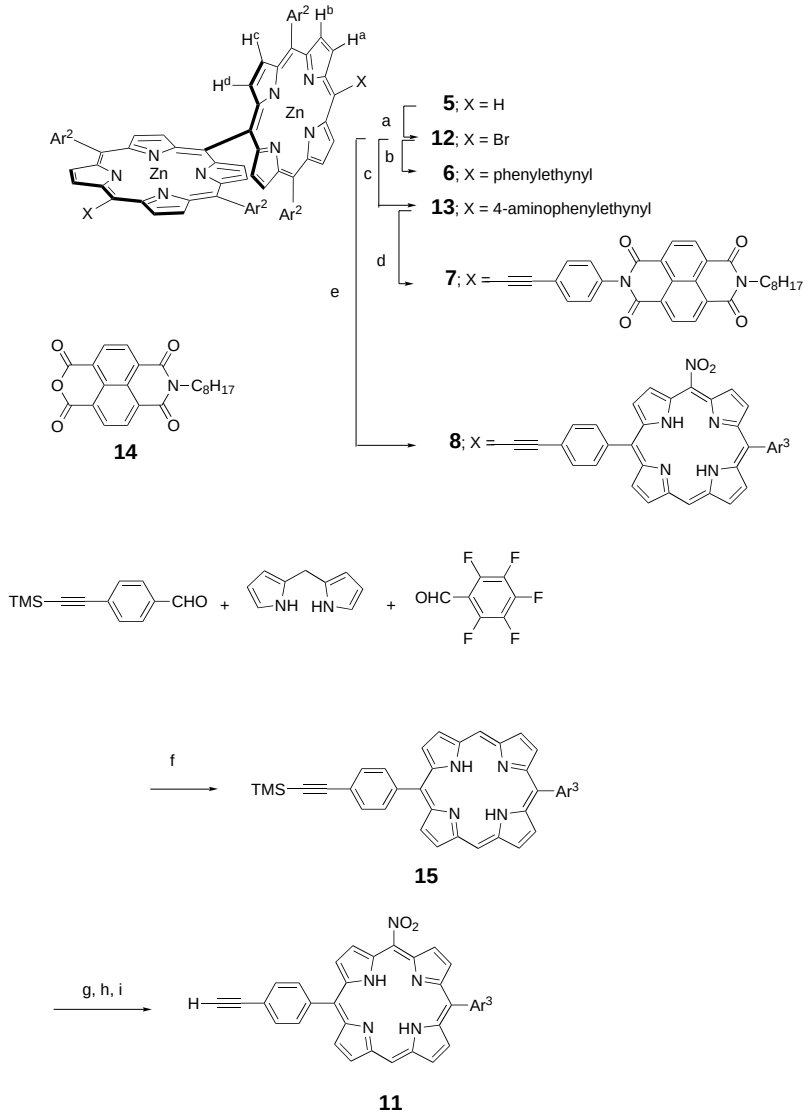

Scheme 1. Synthesis of *meso,meso*-modified porphyrin dimer. $Ar^2 = 3,5$-di-*tert*-butylphenyl, $Ar^3 = 2,3,4,5,6$-pentafluorophenyl, a) NBS, $CHCl_3$, pyridine, 79%; b) phenylacetylene, $[Pd(PPh_3)_2Cl_2]$, CuI, toluene, Et_3N, 70%; c) 4-aminophenylacetylene, $[Pd(PPh_3)_2Cl_2]$, CuI, toluene, Et_3N; d) **14**, pyridine, 41% (two steps); e) **11**, $[Pd_2(dba)_3]$, $AsPh_3$, toluene, Et_3N, 25%; f) TFA, CH_2Cl_2; DDQ, 17%; g) $Zn(OAc)_2$; $AgNO_2$, I_2, $CHCl_3$; h) TBAF, THF; i) 1N HCl, 41% (three steps). dba = dibenzylideneacetone, TBAF = tetrabutylammonium fluoride.

at 530–545 nm into its S_1 state or at 420 nm into its S_2 state. Interestingly, the absorption spectrum of **2** has high absorptivity in a wide range between 380–650 nm, and is thus quite suitable for capturing sunlight.

The steady-state fluorescence spectra of **2, 6**, and **9** are shown in Figure 3b. In spite of the selective excitation into the S_1 state of the peripheral porphyrin at 545 nm, the steady-state fluorescence of **2** was practically the same as that of **6**(D), indicating the near complete energy transfer from the peripheral porphyrins to the modified diporphyrin core. On the basis of the absorption and fluorescence spectra of **6**, the energy level of the S_1 state of D has been estimated to be 1.92 eV. Therefore, the modified windmill porphyrin array **2** has an energy difference of 0.21 eV which is thus larger than that of 0.06 eV in **1**, and is therefore favorable for the intramolecular energy transfer. In addition, the donor emission and acceptor absorption in **2** overlap very well, and the spectral overlap is apparently larger than that in **1** (Figure 4), thus making the rapid energy transfer favorable.

The absorption spectra of the models **3** and **4** are similar to that of **2** except the absorbances due to NI and F and the resultant exciton coupling, particular in the case of **4** (Figure 5a), while the fluorescence intensities of **3** and **4** were extremely weak, and the relative intensities with respect to **2** were less than 0.02 as shown in Figure 5b.

Estimation of energy levels

The energies of the excited states have been determined from the fluorescence and absorption (0,0) bands. For estimation of the energy level of the ion-pair states, one-electron oxidation and reduction potentials were measured by using cyclic voltammetry or differential pulse voltammetry in PhCN. The one-electron oxidation potentials of **6**, **7**, and **9** are 0.32, 0.34, and 0.16 V, respectively, and the one-electron reduction potentials of NI and the free-base porphyrin reference **11** are -0.99 and -1.10 V versus ferrocene/ferrocenium ion couple, respectively. From these E_{ox} and E_{red} values, the energy levels of the ion-pair states were estimated with the corrected solvation energies according to the Born equation (1).[21]

$$E(IP) = E_{ox} - E_{red} + \frac{e^2}{2}\left(\frac{1}{r_D} - \frac{1}{r_A}\right)\left(\frac{1}{4\pi\varepsilon_0\varepsilon} - \frac{1}{4\pi\varepsilon_0\varepsilon_r}\right) - \frac{e^2}{4\pi\varepsilon_0\varepsilon R_{DA}} \qquad (1)$$

E_{ox} and E_{red} are the oxidation and reduction potentials of the donor and acceptor, respectively, measured in PhCN, r_D and r_A are the effective radii of the donor cation and acceptor anion (P^+, 5.5 Å; D^+, 8.0 Å; NI^-, 3.5 Å, F^-, 5.5 Å), respectively, ε_r and ε are dielectric constants of PhCN (25.20) and THF (7.58), respectively, R_{DA} is the separation between the opposite charges estimated from MM2 calculation, 15.3 Å for P-D^+-NI^- and 19.1 Å for P^+-D-NI^- in **3**, and 19.2 Å for P-D^+-FB^- and 19.5 Å for P^+-D-F^- in **4**, respectively. Importantly, there are favorable energy gradients in the order of ^{1}P*-D-NI (2.13 eV) > P-^{1}D*-NI (1.92 eV) > P-D^+-NI^- (1.50 eV) > P^+-D-NI^- (1.36 eV), and ^{1}P*-D-F (2.13 eV) >

© WILEY-VCH Verlag GmbH, D-69451 Weinheim, 2001
0947-6539/01/0714-3138 $ 17.50+.50/0 *Chem. Eur. J.* **2001**, *7*, No. 14

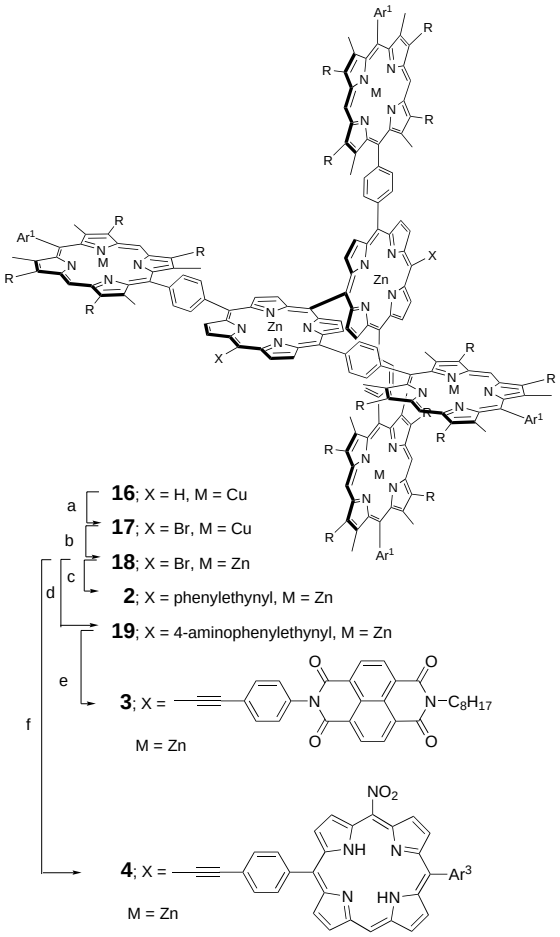

Scheme 2. Synthesis of *meso,meso*-modified windmill porphyrin models. $Ar^1 = 3,5$-di-octyloxyphenyl, $Ar^3 = 2,3,4,5,6$-pentafluorophenyl, $R = C_6H_{13}$, a) NBS, $CHCl_3$, pyridine; b) TFA, 10% H_2SO_4, CH_2Cl_2; $Zn(OAc)_2$, 95% (two steps); c) phenylacetylene, $[Pd(PPh_3)_2Cl_2]$, CuI, toluene, Et_3N, 33%; d) 4-aminophenylacetylene, $[Pd(PPh_3)_2Cl_2]$, CuI, toluene, Et_3N; e) **14**, pyridine, trace (two steps); f) **11**, $[Pd_2(dba)_3]$, $AsPh_3$, toluene, Et_3N, 23%.

P-^{1}D*-F (1.92 eV) > P-D$^+$-F$^-$ (1.52 eV) > or P$^+$-D-F$^-$ (1.40 eV) predicted for **3** and **4**, encouraging coupled energy transfer and electron transfer relay like those found in natural photosynthesis.

Photoexcited-state dynamics of 6

The picosecond time-resolved fluorescence spectra indicated time-dependent fluorescence spectral changes for **6** (Figure 6a). The fluorescence spectrum observed immediately after the laser excitation was sharp with a peak at 632 nm and gradually changed to a broad and red-shifted spectrum, and finally became identical to the emission spectrum of the steady-state fluorescence ($\lambda_{max} = 655$ nm) which decayed with $\tau = 1.48$ ns at room temperature. This spectral change proceeded with $\tau \approx 20-30$ ps but could not be reproduced satisfactorily with a single exponential function. The similar time-dependent fluorescence spectral changes were observed for **20** and also for the core diporphyrin subunit (D) in **2**, but not for **5**, **21**, **22**, or **23**. Interestingly the time-resolved

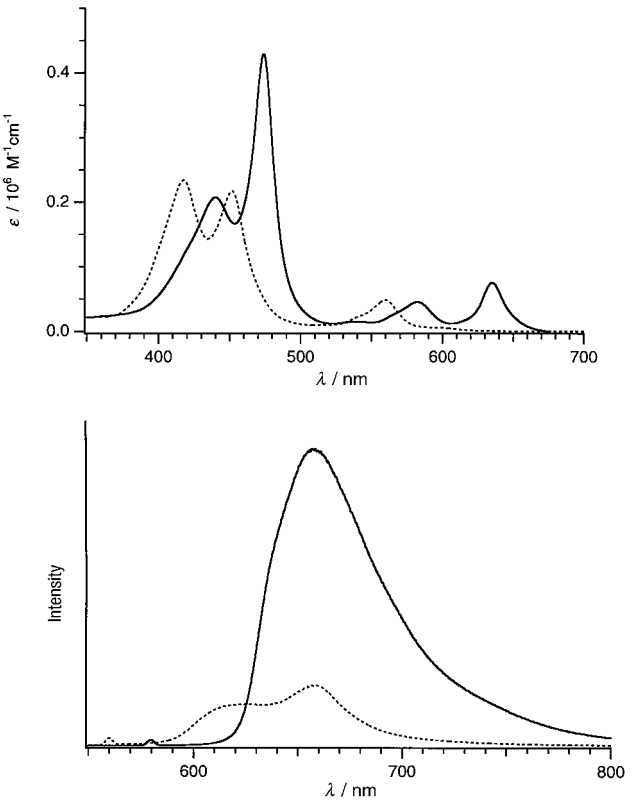

Figure 1. Absorption (top) and fluorescence spectra (bottom) of **5** (dotted, $\lambda_{ex} = 565$ nm) and **6** (solid, $\lambda_{ex} = 580$ nm) in THF.

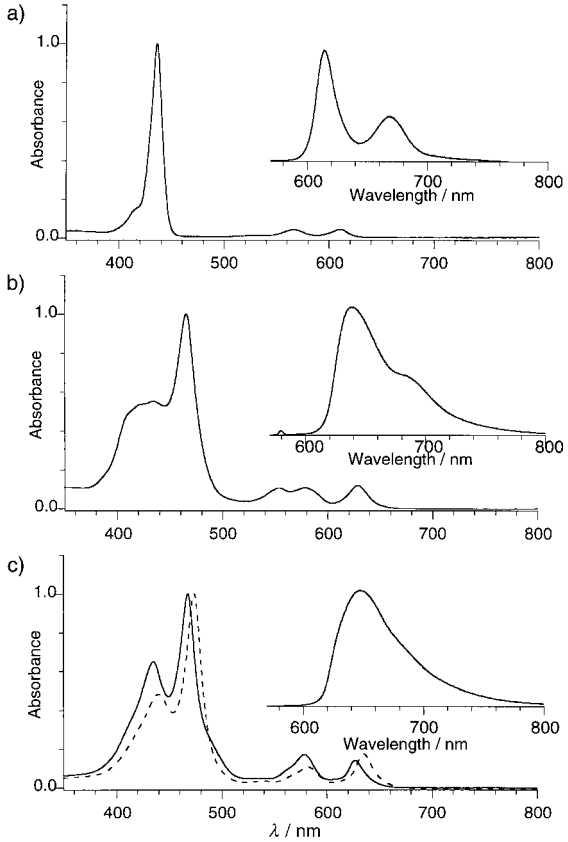

Figure 2. Absorption and fluorescence spectra (inset) of a) **23** ($\lambda_{ex} = 565$ nm), b) **21** ($\lambda_{ex} = 580$ nm), and c) **20** ($\lambda_{ex} = 550$ nm) in THF. Absorption spectrum of **6** is also shown as a dotted line for comparison (c).

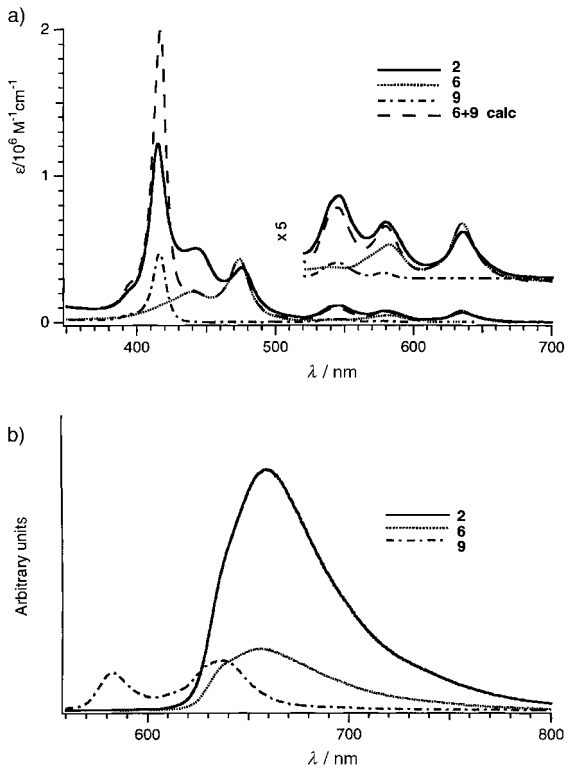

Figure 3. a) Absorption spectra of **2** and its references (**6**, **9**) in THF. A sum of the absorption spectra (**6** and $4 \times$ **9**) was also shown for comparison. b) Fluorescence spectrum of modified windmill porphyrin array **2** taken in THF for excitation at 550 nm. Fluorescence spectra of **6** ($\lambda_{ex} = 580$ nm) and **9** ($\lambda_{ex} = 545$ nm) are shown for comparison. Concentrations are 1×10^{-6} M for **2** and **6** and 4×10^{-6} M for **9**.

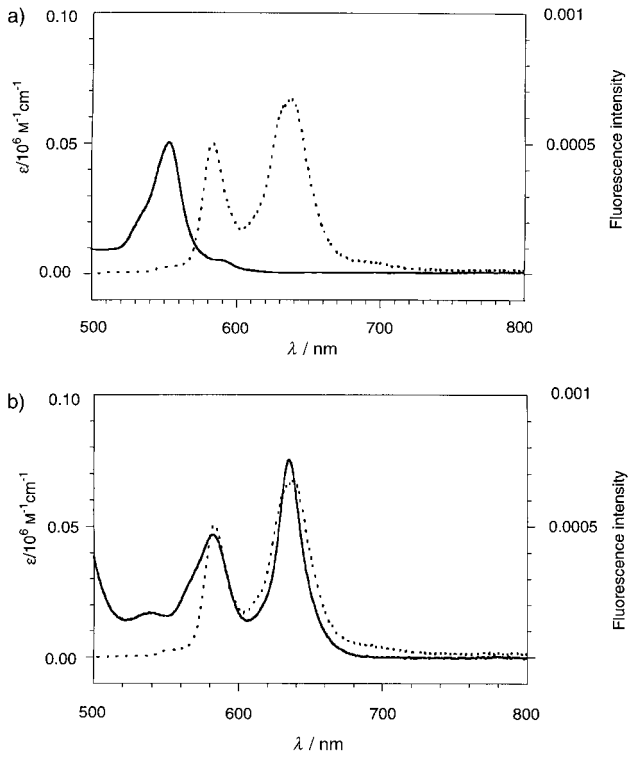

Figure 4. Spectral overlap between the fluorescence (dotted line) of the peripheral porphyrin donor and the absorbance of the central diporphyrin acceptor (solid line): a) **1**, the fluorescence spectrum of **9** versus the absorption spectrum of **5**; b) **2**, the fluorescence spectrum of **9** versus the absorption spectrum of **6**.

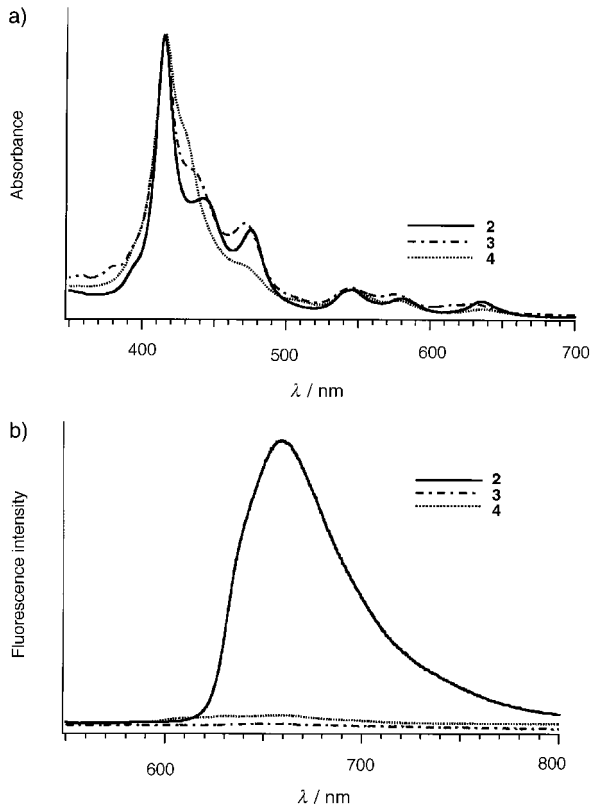

Figure 5. Absorption spectra (a) and fluorescence spectra (b) of **2**, **3**, and **4** ($\lambda_{ex} = 545$ nm) in THF. The absorption spectra are normalized at 415 nm.

fluorescence spectra of **6** in a frozen MTHF matrix at 77 K (Figure 6b) did not exhibit such remarkable spectral changes.

Transient absorption spectroscopy was also employed for the direct detection of the temporal evolution of **6** in the early excitation. Figure 7a shows the time-resolved transient absorption spectra of **6** in THF taken for excitation with a 532-nm laser pulse with a fwhm of 15 ps. The spectrum immediately after excitation (delay time of 0 ps) exhibited the bleaching signals at 583 and 640 nm, which were assigned to the depletion of the ground state of **6**. In addition to these two signals, a broad and shallow dip around 705 nm was observed. This dip is attributable to the induced emission of the S_1 state of **6**. The absorption around 660 nm, which shows a positive value after the excitation, evolves in time into a negative signal in the several tens of picosecond time region. The absorption signal around 660 – 750 nm at a delay time of 85 ps, at which the rapid relaxation was completed, was attributed to the induced emission of the relaxed S_1 state of **6**. With further increase in the delay time, the absorption spectrum gradually changes its shape with a time constant of 1.48 ns, which is in agreement with the fluorescence lifetime.

To more precisely obtain the temporal behavior in the early stage after excitation, femtosecond transient absorption measurements were applied. Figure 7b shows the time profile at 680 nm following the excitation with a 640 nm laser pulse with a fwhm of 150 fs. The rapid appearance of the positive absorption signal is followed by rapid decay into negative absorbance, and gradual recovery of this negative signal was observed in a time region of a few hundreds of picoseconds.

© WILEY-VCH Verlag GmbH, D-69451 Weinheim, 2001
0947-6539/01/0714-3140 $ 17.50+.50/0 *Chem. Eur. J.* **2001**, *7*, No. 14

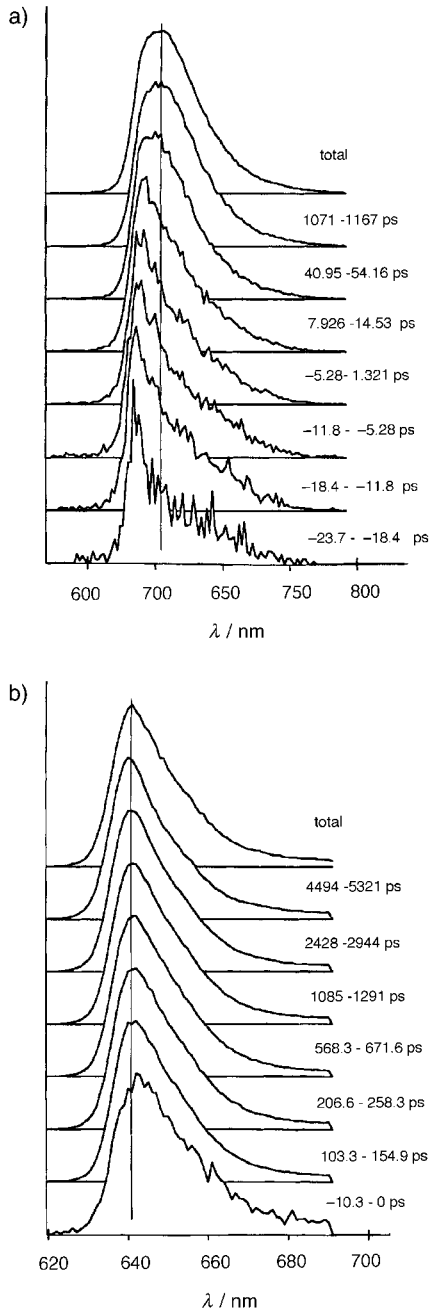

Figure 6. Time-resolved fluorescence spectra of **6;** a) ($\lambda_{ex} = 420$ nm) in THF at room temperature, and b) ($\lambda_{ex} = 440$ nm) in 2-methyltetrahydrofuran at 77 K.

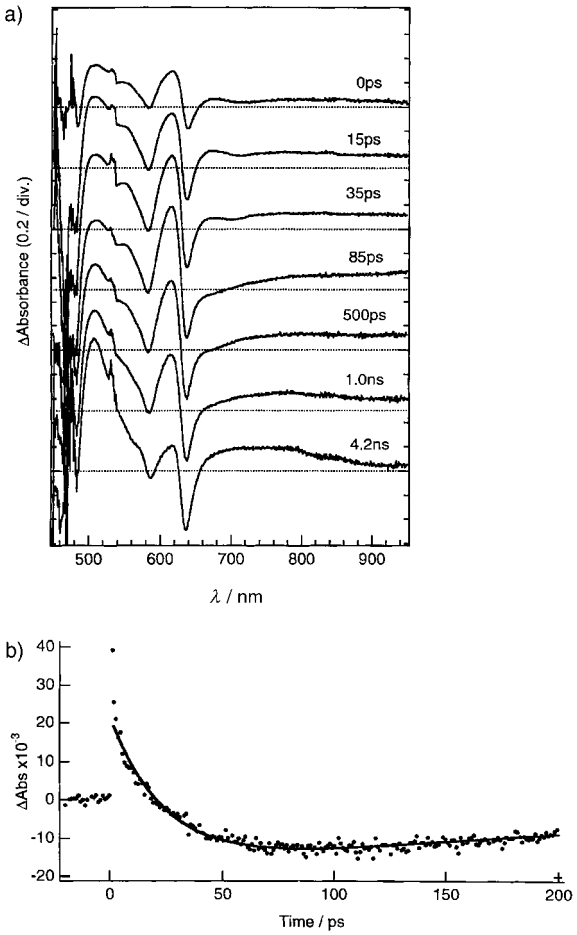

Figure 7. Transient absorption spectra of **6** in THF; a) the transient absorption spectra at different delay times measured by a ps laser system ($\lambda_{ex} = 532$ nm); b) time profile at $\lambda_{pr} = 680$ nm measured by a fs laser system ($\lambda_{ex} = 640$ nm) and fitting curve with 24–26-ps decay and 1.48-ns rise components.

The solid line represents the calculated curve based on a biexponential function with a 26-ps decay component and a 1.48-ns rise component. As shown in Figure 7b, the rapid decay was not perfectly reproduced by the exponential process. As will be discussed later, the fast component immediately after excitation may be related with the distribution of the dihedral angel between the porphyrin moieties.

In line with the time-resolved fluorescence studies, **5**, **21**, **22**, and **23** did not exhibit similar spectral changes in the transient absorption spectra to those of **6**, whereas **20** showed similar behavior to **6** with a similar time constant (ca. 25 ps).

Photodynamics of 2; efficient energy transfer both in S_1 state and S_2 state

The initial motivation of the *meso,meso′*-bisphenylethynylation was to enhance the $S_1 - S_1$ energy transfer from P to D by decreasing the energy level of the S_1 state of D as well as by increasing the spectral overlap integral associated with the intramolecular energy transfer. As described above, the steady-state fluorescence spectrum of **2** displayed only the emission from D, indicating almost quantitative energy transfer. Measurement of the fluorescence decay of P in **2** using a picosecond time-correlated single-photon counting apparatus[22] indicated a lifetime of less than 10 ps. The fluorescence emission at 660 nm, at which the fluorescence is largely attributed to the relaxed $^1D^*$, could be reproduced with a biexponential function with a 13-ps rise component and a 1.39-ns decay component. But lifetimes of about 10–13 ps were very close to or almost shorter than the instrumental limit of the picosecond transient absorption spectroscopy set-up. We thus employed the femtosecond fluorescence up-conversion method[23] to obtain a more accurate rate constant for the energy transfer in **2**. Figure 8 shows the fluorescence

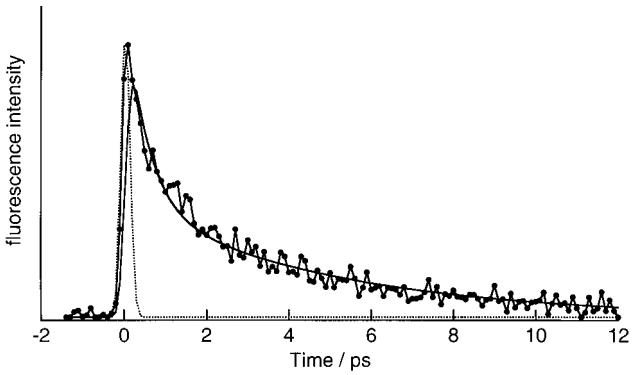

Figure 8. Fluorescence decay curve of **2** at 585 nm measured with the femtosecond up-conversion method ($\lambda_{ex} = 420$ nm) in THF. Dashed line shows the instrumental response function.

decay of **2** at 585 nm recorded for excitation at 420 nm measured by the up-conversion method, which could be reproduced with a biexponential function with time constants of 0.52 ps (63 %) and 4.9 ps (37 %). The faster component was assignable to the vibrational relaxation of the S_1 state of the zinc(II) β-octaalkylporphyrin on the basis of previous studies in which similar time constants were found for the vibrational relaxation of the reference zinc(II) β-octaalkylporphyrin monomer.[23] Therefore, the slower time constant, 4.9 ps, was assigned to the intramolecular energy transfer and this time constant corresponded to 99.6 % efficiency for the energy transfer.

The intramolecular energy transfer in **2** was also examined by the picosecond- and femtosecond-time-resolved transient absorption spectroscopy. Figure 9 shows the transient absorption spectra of **2** measured by the picosecond laser system[24] with an excitation at 532 nm which corresponds to the selective population of ^{1}P*. The transient absorption spectrum at a delay time of 10 ps showed relatively large bleachings at 545 and 580 nm due to the formation of ^{1}P*, but bleaching at 645 nm, which was ascribed to formation of ^{1}D*, was not negligible probably due to the very rapid energy transfer. By increasing the delay time from 10 ps to 40 ps and 100 ps, the contribution of ^{1}P* to the overall transient spectrum diminished and the contribution of ^{1}D* increased. To determine a more accurate rate of the energy transfer, we measured the time profiles at 545 and 645 nm by using femtosecond-time-transient absorption spectroscopy (Figure 10). The bleaching due to ^{1}P* at 545 nm was recovered with a time constant of 3.2 ps, and at the same time the bleaching due to ^{1}D* at

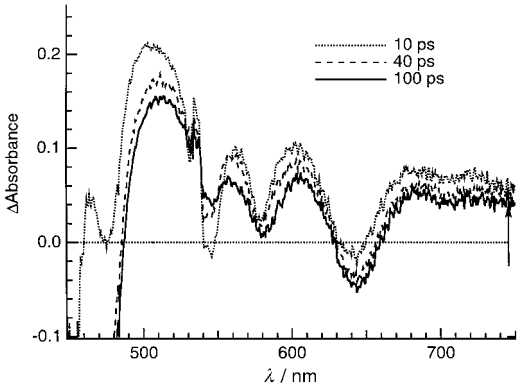

Figure 9. Transient absorption spectra of **2** in THF measured by ps laser system ($\lambda_{ex} = 532$ nm).

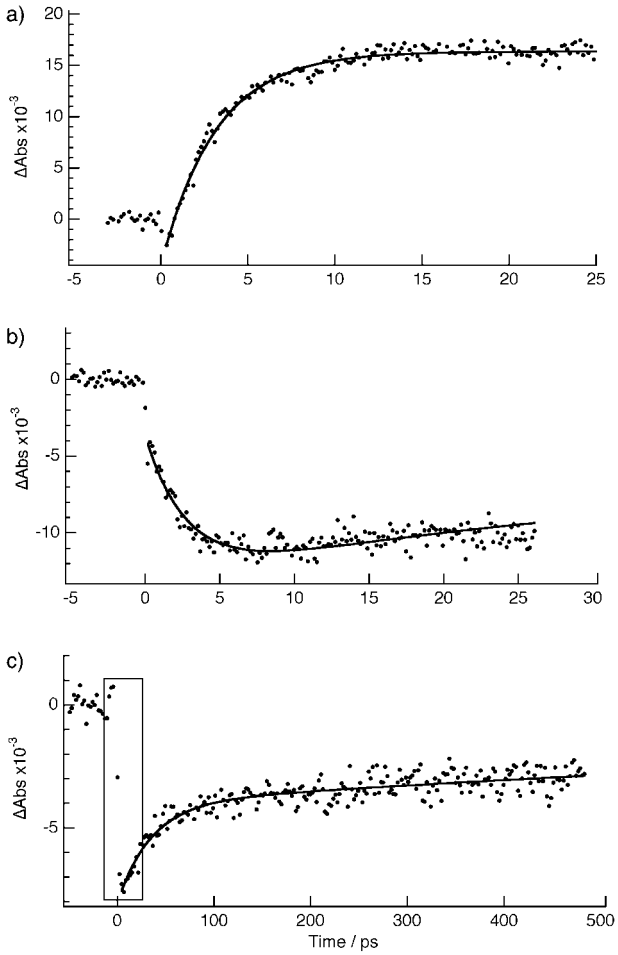

Figure 10. Time profile of transient absorption spectra of **2** in THF measured by fs laser system ($\lambda_{ex} = 545$ nm); a), $\lambda_{pr} = 545$ nm, fitting curve with 3.2-ps rise; b), $\lambda_{pr} = 645$ nm, fitting curve with 2.8-ps decay; c), $\lambda_{pr} = 645$ nm, fitting curve with 35-ps and 1.45-ns rise components.

645 nm increased with a time constant of 2.8 ± 0.4 ps. In a shorter time scale, the bleaching at 645 nm was recovered with time constants of 35 ps and 1.45 ns. The time constant of 1.45 ns was assigned to the fluorescence lifetime, while the shorter 35-ps constant may be attributed to some structural relaxation of the central diporphyrin unit as was observed in Figure 7. On the basis of a time constant of about 3.0 ps, the rate of the energy transfer in the S_1 state, k_{E1}, was calculated as 3.3×10^{11} s^{-1} by using Equation (2), in which τ and τ_0 are the lifetime of the S_1 state of D in **2** and the fluorescence lifetime of the reference molecule **9** (1.3 ns), respectively.

$$k_{E1} = \tau(S_1)^{-1} - \tau_0(S_1)^{-1} \quad (2)$$

We also examined the possibility of energy transfer from P to D in the S_2 state manifold. In the case of **2**, the energy donor is a zinc(II) 5,15-diaryl β-octaalkyl-substituted porphyrin (P), for which we have identified the S_2 state fluorescence

© WILEY-VCH Verlag GmbH, D-69451 Weinheim, 2001
0947-6539/01/0714-3142 $ 17.50+.50/0 *Chem. Eur. J.* **2001**, *7*, No. 14

emission centered at about 423 nm and the fluorescence lifetime to be as short as 150 fs by the fluorescence up-conversion measurement,[23] while the energy acceptor is D, which exhibits S_2 absorption bands at 442 and 476 nm. The Soret band at 442 nm nicely overlaps with the S_2 emission of P, ensuring the large spectral overlap. In the up-conversion measurement, we used benzene instead of THF as the solvent to compare the photoexcited state dynamics of **6** with our recent results[23] and also to suppress the effect of the solvation dynamics in the ultrafast time region, since the interaction of an excited molecule with solvent would be smaller for less polar solvents. After the acceptor-free reference molecule **10** was excited with the second harmonic of the Ti:sapphire laser at 390 nm into the selective population of the S_2 state, the emission decays at 430 and 580 nm (corresponding to the S_2 and S_1 fluorescence) were monitored by the up-conversion method. The fluorescence decay at 430 nm was represented by a single exponential function with $\tau = 150 \pm 10$ fs and that at 580 nm was represented by a sum of a 150-fs rise and 1.5-ns decay in accord with the previous study.[23] In a similar manner, **2** was excited with 390-nm light into the S_2 state of the P, and the emission at 430 nm corresponding to the S_2 fluorescence of P was monitored (Figure 11). The fluorescence signal at 430 nm decayed with $\tau = 68$ fs, and this lifetime was distinctly shorter than the corresponding decay of the acceptor-free reference compound **10**, suggesting energy transfer from the S_2 state of the P. When we assume that this decrease of the S_2 fluorescence lifetime is due to S_2–S_2 energy transfer, the rate of the energy transfer, k_{E2}, is calculated to be $8 \times 10^{12}\ s^{-1}$ [Eq. (3)].

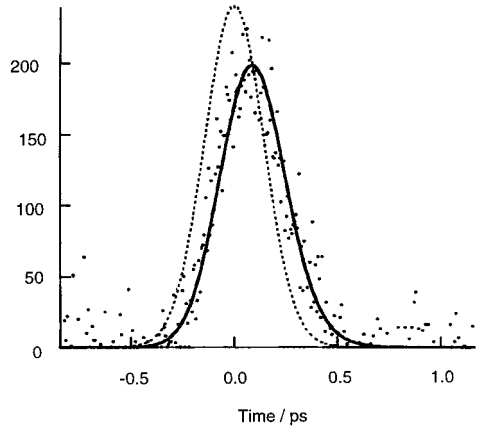

Figure 11. Fluorescence up-conversion results of **2** in benzene, $\lambda_{ex} =$ 388 nm and $\lambda_{em} = 430$ nm.

$$k_{E2} = \tau(S_2)^{-1} - \tau_0(S_2)^{-1} \quad (3)$$

Photoinduced electron-transfer reactions in 7 and 3

The fluorescence spectra of NI-linked models **7** (not shown) and **3** (Figure 5b) were almost completely quenched. The transient absorption spectra of **7** (Figure 12a) revealed an immediate rise and a slower decay both in the sharp absorption band at 610 nm and the broad absorption band at around 710 nm. At a delay time of 100 ps, these absorbances were almost gone, indicating that the transient species formed upon photoexcitation have lifetimes of less than 100 ps. The electron-acceptor NI moiety was employed as an acceptor unit because of its characteristic absorption,[19, 25] but the transient absorption bands due to the cation radical and the S_1 state of zinc(II) bisphenylethynylated diporphyrin display conisderable overlap with the absorption bands (480, 610, 770 nm) of NI^-. Nevertheless, the transient spectra in Figure 12a showed the absorbances at 490 and 610 nm and the strong bleaching at 590 and 640 nm and thus could be assigned to the ionic species D^+-NI^-, since the spectra were entirely different from the transient absorption spectrum of $^1D^*$. Femtosecond laser spectroscopy was applied to obtain precise data regarding the time dependence of the transient absorption spectra with higher time resolution. The time profile of the transient absorbance at 690 nm was analyzed in terms of 10-ps rise and 26-ps decay time constants (Figure 12b). Since the 26-ps decay time constant was similar to its fluorescence lifetime (25 ps), this time constant was assigned to the charge-separation process. The other 10-ps rising time constant was

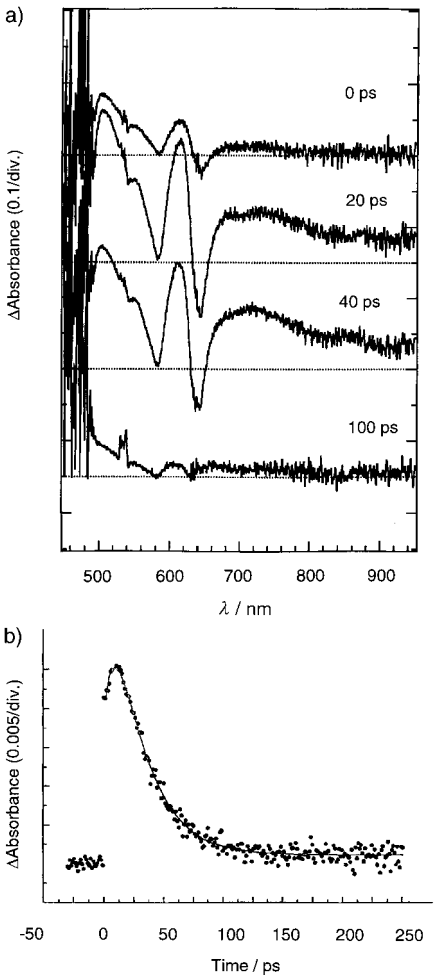

Figure 12. Transient absorption spectra of **7** in THF. a) Spectra with ps laser system, $\lambda_{ex} = 532$ nm. b) Time profile with fs laser system, $\lambda_{ex} =$ 640 nm, $\lambda_{pr} = 690$ nm, fitting with 10-ps rise and 25-ps decay components.

therefore assigned to the charge recombination of D^+-NI^- to the ground state. Thus, the electron-transfer reactions in **7** can be summarized by the charge separation of $^1D^*$-NI $\rightarrow$ D^+-NI^- with $\tau = 25$ ps and the charge recombination of D^+-NI^- $\rightarrow$ D-NI with $\tau = 10$ ps. The faster charge recombination is evidently unfavorable for the overall charge-separation processes.

Figure 13 shows the transient absorption spectra of **3**. The charge-separated state P^+-D-NI^- is probably represented by the transient absorption spectrum with a delay time of about

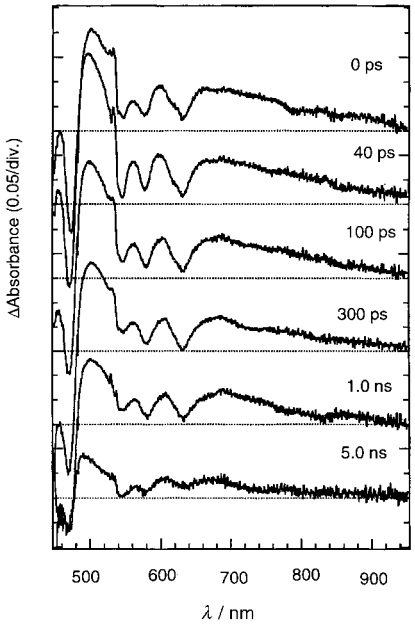

Figure 13. Transient absorption spectra of **3** in THF. $\lambda_{ex} = 532$ nm.

300 ps and decayed with $\tau = 3$ ns. Although the lifetime of P^+-D-NI^- was actually longer than that (10 ps) of P-D^+-NI^- in accord with the longer distance between the charged sites in the former ion pair, the overall quantum yield for the formation of P^+-D-NI^- was rather low, judging from the small absorbance of the transient absorption spectra.

Photoinduced electron-transfer reactions in 8 and 4

The absorption spectrum of the reference diporphyrin **8** (not shown) can be roughly described as the sum of those of **6** and **11** but is considerably broader, indicating substantial electronic interactions between D and F. Since the energy level of the S_1 state of F (1.93 eV) is nearly the same as that of D (1.92 eV), there may be rapid energy transfer between D and F but the fluorescence is strongly quenched in THF, indicating the efficient charge separation. The fluorescence of **8** exhibited a single exponential decay with $\tau = 12$ ps. The electron-transfer reactions in **8** were studied by transient absorption spectroscopy (Figure 14), which showed the formation and decay of an ion-pair state similar to the case of **7**. In the case of **8**, the absorbance at around 690 nm was stronger due to the superposition of the absorption band of F^- on that of D^+.[15] This characteristic absorbance band increased with $\tau = 10$ ps and decayed with $\tau = 55$ ps. The shorter

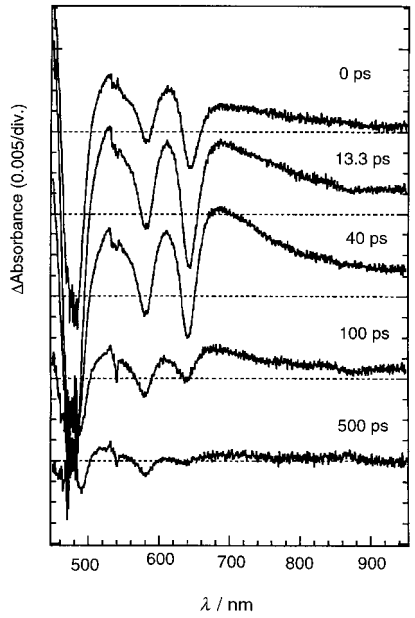

Figure 14. Transient absorption spectra of **8** in THF. $\lambda_{ex} = 532$ nm.

time constant of 10 ps was similar to the fluorescence lifetime and thus was assigned to the charge separation, and the slower time constant of 55 ps was assigned to the charge recombination. In summary, the change of the electron acceptor from NI to F led to the increase in the rate of the charge separation from 25 ps^{-1} to 10 ps^{-1} and also the decrease in the rate of the charge recombination from 10 ps^{-1} to 55 ps^{-1} as expected.

Figure 15 shows the transient absorption spectra of the porphyrin octameric model **4**. The spectrum at a delay time of 40 ps revealed absorbances at 495, 610, 680, and 910 nm and

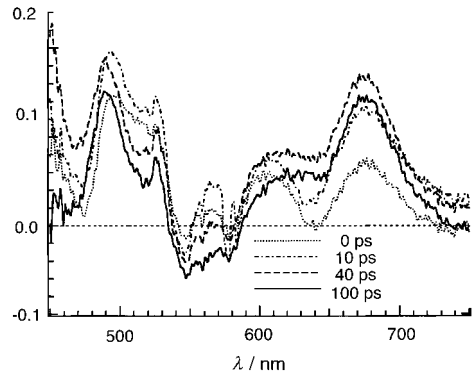

Figure 15. Transient absorption spectra of **4** in THF. $\lambda_{ex} = 532$ nm.

bleachings at 550 and 580 nm. The positive absorbances at 495, 680, and 910 nm were assigned to F^-, and a broad band at 600 – 700 nm was assigned to P^+, and the bleachings were due to the depletion of the ground state P, presenting evidence for formation of P^+-D-F^-. These transient absorbances decayed with $\tau = 3$ ns. Although the accurate determination of the amounts of the final charge-separated states has not been accomplished yet, it is clear that the transient absorbance due to the ionic product is larger in **4** than in **3**.

© WILEY-VCH Verlag GmbH, D-69451 Weinheim, 2001
0947-6539/01/0714-3144 $ 17.50+.50/0 *Chem. Eur. J.* **2001**, *7*, No. 14

Discussion

As reported previously, the windmill porphyrin arrays have a nice architecture as a light-harvesting antenna functional unit in light of their three-dimensionally extended structure as well as the exothermic energy gradient from the peripheral porphyrins to the *meso*–*meso*-linked diporphyrin core. Major aims of the work described herein are through appropriate molecular modifications, 1) to enhance the efficiency of the intramolecular energy transfer from the peripheral porphyrins to the *meso*–*meso*-linked diporphyrin core, 2) to couple the energy transfer and charge-separating functional units, and 3) to achieve favorable overall charge separation with high quantum yield. The *meso*,*meso*′-bisphenylethynylation of the parent windmill porphyrin array **1** meets these requirements, since 1) it lowers the energy level of the resultant *meso*,*meso*′-bisphenylethynylated *meso*–*meso*-linked diporphyrin core so that the intramolecular energy transfer is made very efficient and one-directional, 2) it extends the electronic orbitals of the diporphyrin chromophore to the two phenylethynyl substituents, thus facilitating rapid electron transfer from the modified diporphyrin core to the attached electron acceptor, and 3) it allows the easy synthetic attachment and tuning of an electron acceptor for the formation of long-lived charge separated state.

Exciton coupling among porphyrin arrays: First the absorption and fluorescence properties of the modified windmill porphyrin array **2** are worthy of discussion.[13-26] The split Soret bands in **5** can be qualitatively explained by the simple point-dipole exciton coupling theory developed by Kasha.[27] The Soret band of a zinc(II) porphyrin monomeric unit has two perpendicular, components b_X and b_Y, which are parallel and perpendicular, respectively, with respect to the direction of the *meso*–*meso* connection. In a simple monomer, they are degenerate, but in a porphyrin dimer they couple differently. When we assume an averaged perpendicular conformation of **5**, which is predicted to be most stable on the basis of the AM1 calculation,[26b,c] only the b_x transitions are parallel, and the other dipole interactions should be zero (Scheme 3). Dipole transitions are allowed to the lower energy of the two b_X states and the two unperturbed transitions b_Y and b_Z. Therefore, we assigned the low-energy split Soret band to the exciton-coupled transition b_x+b_x and the high-energy split Soret band to the residual monomeric Soret band transition b_y, b_z. This assignment has been further supported by fluorescence anisotropy and resonance Raman measurements.[26b,c]

On the other hand, the absorption spectrum of **6** can be explained in an analogous manner to that of **5**, except for the fact that *meso*-phenylethynylation led to the lowering of the near D_4 symmetry of the zinc(II) porphyrin monomeric unit and thus the enhancement and red-shift of the Q band absorption. On the basis of the perpendicular conformation of the two porphyrin rings of **6** as assumed for **5**, the dipole moments (B_x) along the long molecular axis are coupled to result in the absorption band at 474 nm ($B_x + B_x$), while the dipole moments (b_y, b_z) perpendicular to the long axis cannot be coupled with each other to maintain the absorption band at 440 nm, which is near the Soret band of the corresponding monomer **23** (436 nm) but is much broader. The split Soret bands at the high-energy side of **6**, **20**, and **21** were considerably broader in comparison to that of **5**. This may be explained as assuming a wide distribution of conformers with regard to the orientation of the *meso*-ethynyl substituent with respect to the porphyrin plane. The ground-state conformation of the *meso*–*meso*-linked diporphyrin seems to be perpendicular, but the *meso*-ethynyl substituent should be more flexible for its rotation. Since the electronic system of the porphyrin can be considered to extend well to the *meso*-ethynyl substituent, the conformation of this substituent will affect the optical properties of the porphyrin. In line with this consideration, the fluorescence excitation spectra of **6**, **20**, and **21** in the frozen matrix revealed the presence of several conformers which emitted at different wavelengths.

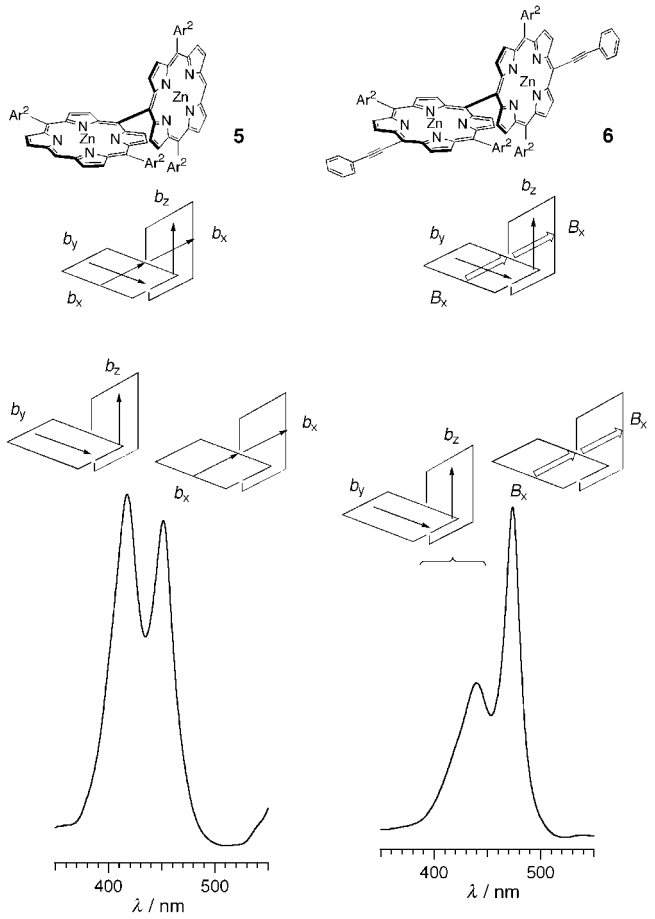

Scheme 3. Assignment of the absorption bands of **5** and **6**.

As described above, the exciton coupling between the peripheral porphyrins and the modified diporphyrin core in **2** is not strong enough to induce the band splitting but certainly large enough to induce the broadening at the Soret band. Considering the fact that two zinc(II) porphyrins bridged by the same 1,4-phenylene spacer exhibited split Soret bands due to exciton coupling,[28] the relatively small exciton interaction in **2** with the same 1,4-phenylene spacer may be ascribed to the nonresonant situation of the two interacting chromophores, P and D, due to the energy difference of the S_2 state.

Dynamic aspects of molecular structure. The modified *meso*–*meso*-linked diporphyrin core **6** (D) displayed unique time-dependent spectral changes both in the time-resolved fluorescence and absorption spectra with $\tau \approx 25-30$ ps. The observed time-dependent red-shift of the fluorescence suggested some energetic relaxation. To explain the transient absorption spectra shown in Figure 7a, we needed at least three states, which were most probably the Franck–Condon S_1 state (S_1'), the relaxed S_1 state (S_1^0), and the T_1 state. We assigned the spectrum at a delay time of 0 ps to the S_1' state, that at a delay time of 85 ps to the S_1^0 state, and that at a delay time of 4.2 ns to the T_1 state. The time constant of 26 ps, assigned to the relaxation from the S_1' state to the S_1^0 state, is somewhat longer than that typical for excited-state vibrational relaxation in porphyrins.[29] The fact that only **6** and **20** displayed these spectral changes indicates that a structural motif of *meso*,*meso*′-diethynylated *meso*–*meso*-linked diporphyrin is indispensable for these spectral changes. One possible explanation for this spectral change is a conformational rotation around the *meso*–*meso* C–C bond during the relaxation in the S_1 state manifold. In the parent *meso*–*meso*-linked diporphyrin **5**, rotation about the *meso*–*meso* C–C bond is expected to be substantially hindered, and the coplanarity of the porphyrin rings cannot be achieved. In fact, the *meso*–*meso*-linked diporphyrin made from 5,15-differently substituted porphyrin was chiral, and its chirality was not lost even upon heating at 147 °C for several hours.[30] The semiempirical AM1 calculation shows that the dihedral angle distribution in **5** is $90 \pm 20^\circ$ at ambient temperature.[26b,c] *meso*,*meso*′-Bisphenylethynylation would have no serious influence on the dihedral angle distribution and thus we may expect a similar dihedral angle distribution for **6** in the ground state. Upon photoexcitation, the immediately formed Franck–Condon state should have a similar perpendicular conformation but would have larger electronic interactions between the porphyrins than those in the ground state. This may induce conformational relaxation towards more planar geometry. In line with this consideration these changes were suppressed in the frozen matrix environment as noted in the previous section. Fluorescence spectral changes were prominent for **6**, **2**, and **20** with a common *meso*,*meso*′-bisethynylated *meso*–*meso*-linked diporphyrin structure. This may indicate that a subtle change in the dihedral angle will lead to larger changes in the optical properties in the case of the *meso*,*meso*′-bisethynylated *meso*–*meso*-linked diporphyrins.

Energy transfer: Generally, the two types of electronic interaction are identified for the energy-transfer processes; one is the Coulombic interaction effected by the through-space coupling of transition dipole moments through an oscillating electromagnetic field[31] and the other is the electron exchange interaction that is provided by direct or indirect overlap of wave functions.[32] These two interactions are considered to be a dominant factor for the Förster and Dexter mechanisms, respectively. As such, the evaluation of the relative contribution of through-space versus through-bond interaction in energy-transfer processes has been important for understanding the mechanism as well as the design of further elaborate energy-transfer molecular devices. In the limit of the weak interactions, the rate constant for the Förster energy transfer is given by Equations (4) and (5), where n is the refractive index of the solvent, R is the center-to-center distance between donor and acceptor, Φ is the fluorescence quantum yield of the donor, κ is a dipole–dipole orientation factor, J is the spectral overlap integral, τ is the fluorescence lifetime of the donor, $F(\nu)$ is the normalized fluorescence spectrum of the energy donor, and $\varepsilon(\nu)$ is the absorption spectrum of the energy acceptor with molar extinction coefficient ($M^{-1}cm^{-1}$) unit.[31]

$$k_{EN} = \frac{8.8 \times 10^{-25} \kappa^2 \Phi}{n^4 R^6 \tau} J \quad (4)$$

$$J = \int F(\nu)\varepsilon(\nu)\nu^{-4} d\nu \quad (5)$$

Previously we have reported that the energy transfer from peripheral porphyrin units to the central diporphyrin core in the parent windmill porphyrin array hexamer **1** is reversible, on the basis of the observed biexponential fluorescence decay.[7] In the modified windmill porphyrin array **2**, the energy-transfer efficiency was made one-directional and its rate was significantly enhanced to $2-3$ ps^{-1}, corresponding to an energy transfer efficiency of 99.6 %. On the basis of the absorption and fluorescence spectra shown in Figure 4, the spectral overlap integrals of the Förster formula [Eq. (5)] were calculated to be 3.3×10^{-14} and 5.4×10^{-13} cm^{-6} mmol for **1** and **2**, respectively. Therefore, the enhancement of the energy transfer in **2** can be mostly ascribed to its larger spectral overlap integral in comparison to that in **1**. This in turn indicates that the Coulombic interaction is predominant for the energy transfer.

Usually, the upper excited states such as S_2 are too short lived to be involved in energy-transfer or electron-transfer reactions due to extremely rapid internal conversion to the lowest singlet excited state. In this respect, zinc(II) TPP-type porphyrins are exceptional molecules, since they have long-lived S_2 states ($1-2$ ps) principally due to the large energy gap and poor Franck–Condon factor between the S_2 state and the S_1 state.[33] This property favors for the occurrence of some reactions in their S_2 state, and recently several examples have been reported for photochemical reactions in the S_2 state manifold.[34–36] We note here that the S_2-S_2 energy transfer is strongly suggested for **2**, regardless of the extremely short S_2 lifetime (150 fs) of the octaethylporphyrin (OEP)-type energy donor P, since it has the close proximity of the donor and acceptor that is a prerequisite to S_2-S_2 energy transfer, as well the very favorably matched spectral overlap between the fluorescence emission from the S_2 state of the peripheral zinc(II) OEP-type porphyrin energy donor and the strongly allowed absorption to the S_2 state (Soret transition) of the zinc(II)-modified diporphyrin core.

Electron transfer: The electron-transfer dynamics of **3** are interesting from the viewpoint of the duplication of photosynthetic charge separation, in that **3** constitutes a single molecular photosynthetic model that achieves a coupled light-harvesting and charge separation; 1) the four peripheral zinc(II) porphyrins P act as the singlet energy donor toward D to effect the formation of ^{1}D*, 2) ^{1}D* donates an electron to

© WILEY-VCH Verlag GmbH, D-69451 Weinheim, 2001
0947-6539/01/0714-3146 $ 17.50+.50/0 *Chem. Eur. J.* **2001**, *7*, No. 14

NI to generate the D^+-NI^- ion-pair state, and finally 3) the four P act as an electron donor towards D^+, thereby providing the fully charge-separated state P^+-D-NI^-. These sequential photochemical events have been confirmed by the steady-state and transient spectroscopies noted above. A reaction scheme conceivable for the photodynamics of **3** is shown in Scheme 4. The major drawback in the model **3** is the charge

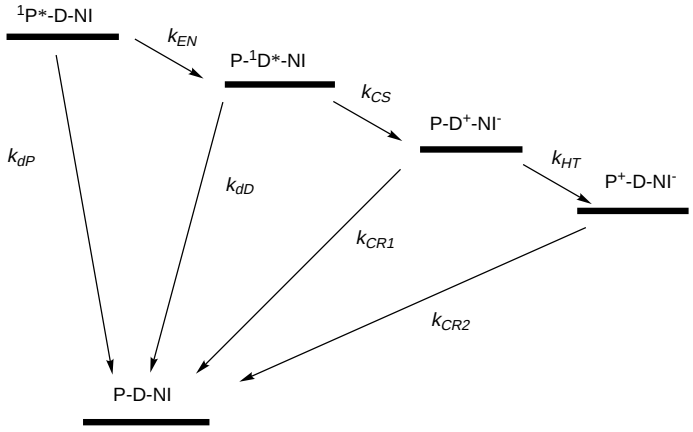

Scheme 4. Energy diagram and reaction scheme of **3**.

recombination reaction (k_{CRI}) in P-D^+-NI^- to reform its ground state which is rapid in comparison to the rate of hole transfer (k_{HT}), leading to a low overall quantum yield for the fully charge-separated state.

In constructing multichromophoric photosynthetic reaction center models capable of charge separation, the adjustment of charge separation (CS) and charge recombination (CR) is always the crucial issue.[3, 4, 6] A key improvement of the overall charge-separation quantum yield in **3** is achieved by the suppression of its fast charge recombination. A starting point for achieving this goal is given by Equation (6), a simple form of the nonadiabatic electron transfer model developed by Marcus.[37]

$$k_{ET} = \sqrt{\frac{\pi}{\hbar^2 \lambda k_B T}} |V|^2 \times \exp\left[\frac{-(\Delta G^0 + \lambda)^2}{4\lambda k_B T}\right] \quad (6)$$

The electron-transfer rate constant k_{ET} is given by the product of a preexponential term and an exponential term. The former includes the matrix element V corresponding to the electronic coupling, and the latter term depends upon the free-energy change for the reaction, ΔG^0, and the reorganization energy, λ. Extensive studies on covalently linked donor–acceptor molecules have revealed that the charge separation always lies in the normal region ($-\Delta G^0 < \lambda$) and the charge recombination always lies in the inverted region ($-\Delta G^0 > \lambda$).[38–42] In this context, an electron acceptor with a similar reduction potential and a smaller λ would be suitable for slowing down the charge recombination. In recent years, it has been revealed that porphyrinic donors and acceptors have smaller values of λ in comparison to those of more compact electron acceptors such as quinones or diimides.[4d,e, 15, 43] Therefore, we employed the porphyrinic electron acceptor F because of the similar reduction potential to NI as well as its expected small reorganization. In addition, the anion radical of F may be detected by transient absorption spectroscopy.[15] On the basis of the Marcus theory [Eq. (6)], the change of the electron acceptor from NI to F may result in faster charge separation as well as retarded charge recombination, hence giving rise to an improvement of the overall charge separation efficiency.

Judicious replacement of NI with F led to enhancement of the charge separation rate (k_{CS}) and to retardation of the charge recombination rate (k_{CR1}), as revealed by transient absorption studies on **4**. Since the values of $-\Delta G^0$ for the initial charge separation are rather similar in **3** (0.42 eV) and **4** (0.40 eV), these results can be understood in terms of smaller values of λ for F in comparison to that for NI. On the basis of the systematic studies on the dependence of the energy gap of the intramolecular CS and CR reactions of porphyrin–quinones[44] and hybrid diporphyrins,[15, 45] the reorganization energy, λ, in **4** is probably substantially smaller than that in **3**. Under these assumptions, the energy gap ($-\Delta G^0$) dependencies of the electron transfer rate can be schematically represented in Scheme 5, in which the bell-shaped parabolas

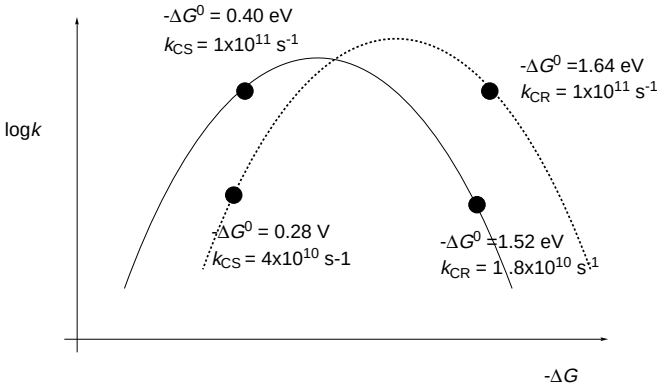

Scheme 5. Schematic representation of Marcus plots for D-NI (dotted line) and D–F (solid line).

are displaced slightly, reflecting a difference in λ, resulting in the relationship of $k_{CS} < k_{CR1}$ in **3** and $k_{CS} > k_{CR1}$ in **4**, although the CS and CR have similar $-\Delta G^0$ values both in **3** and **4**. A similar strategy has been recently employed for enhancing the charge separation efficiency of photosynthetic models.[4d,e, 43]

In summary, the windmill porphyrin arrays are of great interest in view of their architecture, which is favorable for light-harvesting, their good solubility, and the ease of their modification that allows the coupling of the energy transfer and charge separation. New aspects of energy transfer in the S_2 state manifold, and conformation relaxation in the S_1 state of *meso*,*meso'*-bisethynylated *meso*–*meso*-linked diporphyrins are also interesting. Since we have also developed exceptionally large porphyrin array molecules, we aim to apply similar strategies to these giant porphyrin arrays.

Experimental Section

All reagents and solvents were of the commercial reagent grade and were used without further purification except where noted. Dry toluene and triethylamine were obtained by refluxing and distilling over CaH_2. Solvents

used for spectroscopic measurements were all spectra-grade. Preparative separations were performed by silica gel gravity flow column chromatography (Wako, Wakogel C-200), and silica gel flash column chromatography (Merck Kieselgel 60H Art. 7736). Separations of the windmill porphyrin arrays were performed by recycling preparative HPLC (Japan analytical Industry Co., LTD LC-908 with JAIGEL 2.5H, 3H, and 4H columns in series) with $CHCl_3$ as an eluent. Analytical HPLC was performed on JAIGEL-2.5H-AF, 3H-AF and 4H-AF columns in series (eluent, $CHCl_3$; flow rate, 1.2 mL min^{-1}; detected at 400–700 nm) with a JASCO HPLC apparatus using multi-wavelength detector MD915. ^{1}H NMR spectra were recorded in a $CDCl_3$ solution on a JEOL ALPHA-500 spectrometer (operating at 500 MHz), and chemical shifts were represented as δ values in ppm relative to the internal standard of $CHCl_3$ (7.260 ppm). FAB mass spectra were recorded on a JEOL HX-110 spectrometer, using positive-FAB ionization method (accelerating voltage; 10 kV, primary ion sources: Xe) and 3-nitrobenzyl alcohol matrix (3-nba), and matrix-assisted laser desorption ionization time-of-flight (MALDI-TOF) mass spectra were recorded on a KRATOS PC-KOMPACT SHIMADZU MALDI 4 spectrometer using positive-MALDI-TOF method with/without sinapinic acid matrix. UV/Vis absorption spectra were recorded on a Shimadzu UV-2400PC spectrometer. Steady-state fluorescence emission spectra were recorded on a Shimadzu RF-5300PC spectrofluorometer. Redox potential were measured by the cyclic voltammetry method and differential pulse voltammetry method on a ALS electrochemical analyzer model 660.

Fluorescence decay curves and time-resolved fluorescence spectra were measured for 10^{-6}–10^{-7} M air-saturated solutions by using a picosecond time-correlated single photon counting apparatus.[26] A second harmonics of a mode-locked Nd^{3+}:YAG laser (Spectra Physics 3800) at 532 nm or a second harmonic of a Ti:sapphire laser (Coherent MIRA 900) at 410–420 nm was used for the excitation laser pulse. The laser system was combination of a mode-locked Nd^{3+}:YAG laser (Spectra Physics 3800), a pulse compressor (Spectra Physics 3690), and a cavity-dumped DCM laser (Spectra Physics 3500).[22] The fluorescence emission was detected with a micro-channel-plate photomultiplier (Hamamatsu R6890-U). The instrumental response function obtained from scattered light of a vesicle aqueous solution had a width of 30 ps (full width half maximum (fwhm)). Accurate determination of the energy transfer rates was done by using a femtosecond fluorescence up-conversion method based on a Ti:sapphire laser (Spectra Physics, tsunami, 840 nm, 80 MHz) which was pumped with a diode-pumped solid-state laser (Spectra Physics, Millennia X).[23]

Sample solutions with concentrations of 10^{-4}–10^{-5} M were used for transient absorption measurements after nitrogen gas bubbling. Picosecond transient absorption spectra were measured by means of a microcomputer-controlled laser photolysis system with a custom-built repetitive mode-locked Nd^{3+}:YAG laser.[24] The second harmonic of the Nd^{3+}:YAG laser at 532 nm with 15 ps fwhm was used for excitation. For the detection with higher time resolution, a dual OPA femtosecond laser system was employed. The output of Ti:sapphire oscillator (65 fs fwhm, 800 nm, 800 mW, 82 MHz) was regeneratively amplified. This amplified pulse (90 fs fwhm, 1 W, 1 KHz) was divided into two pulses with the same energy and guided into the OPA systems. By using several nonlinear crystals, the OPA can cover the wavelength region from 300 nm to 3 μm with the output energy of a few to several tens of μJ per pulse. One of the two OPA systems was used for the pump light source and the other for the probe pulse. The output energy of the probe pulse was reduced to 1/1000. The pulse duration estimated by the cross-correlation between the pump and probe pulses at the sample position was 160 fs.

Synthesis

***meso,meso′*-Dibrominated *meso*–*meso*-linked diporhyrin 12**: The diporphyrin **5** (88.5 mg, 0.059 mmol) was dissolved in a mixture of $CHCl_3$ (30 mL) and pyridine (0.5 mL). *N*-bromosuccinimide (NBS; 22.5 mg, 0.126 mmol) was added to this solution and the resulting solution was stirred for 10 min at room temperature. The mixture was poured into water and extracted with $CHCl_3$. The combined organic extract was successively washed with water and brine, and dried over Na_2SO_4. After the zinc metalation, the product was purified by silica gel chromatography (eluent CH_2Cl_2) to give **12** (76.9 mg, 46 μmol, 79%). ^{1}H NMR (500 MHz, $CDCl_3$): δ = 9.87 (d, J = 5.0 Hz, 4H; β-H), 9.08 (d, J = 5.0 Hz, 4H; β-H), 8.66 (d, J = 4.5 Hz, 4H; β-H), 8.07 (d, J = 4.5 Hz, 4H; β-H), 8.05 (d, J = 1.5 Hz, 8H; Ar), 7.71 (s, 4H; Ar), 1.45 (s, 72H; *t*Bu); MS (FAB): found 1652, calcd for $C_{96}H_{100}Br_2N_8Zn_2$, 1651.

***meso,meso′*-Bis(phenylethynyl)-substituted *meso*–*meso*-linked diporhyrin 6**: The dibromoporphyrin **12** (13.2 mg, 0.0080 mmol) and phenylacetylene (0.040 mmol) were dissolved in a mixture of toluene (5 mL) and triethylamine (1 mL), and this solution was purged with argon for 30 min. $[Pd(PPh_3)_2Cl_2]$ (4.1 mg) and CuI (3.8 mg) were added, and the resulting solution was heated at 50 °C for 5 h under argon. After the reaction mixture was filtered, chromatography on a silica gel column (eluent CH_2Cl_2/*n*-hexane) gave **6** (9.5 mg, 5.6 μmol, 70%). ^{1}H NMR (500 MHz, $CDCl_3$): δ = 9.95 (d, J = 5.0 Hz, 4H; β-H), 9.11 (d, J = 4.5 Hz, 4H; β-H), 8.66 (d, J = 4.0 Hz, 4H; β-H), 8.11 (d, J = 6.5 Hz, 4H; Ar), 8.09 (m, 4 + 8H; Ar + β-H), 7.73 (m, 4H; Ar), 7.61 (t, J = 7.5 Hz, 4H; Ar), 7.53 (d, J = 7.5 Hz, 2H; Ar), 1.46 (s, 72H; *t*Bu); MS (FAB): found 1699, calcd for $C_{112}H_{110}N_8Zn_2$, 1699; UV/Vis (THF): λ_{max} (logε) = 440 (5.32), 474 (5.63), 583 (4.66), and 635 (4.88) nm; fluorescence (THF): λ_{max} = 657 nm (λ_{max} = 580 nm).

***meso,meso′*-Bis(4-NI-linked-phenylethynyl)-substituted *meso*–*meso*-linked diporphyrin 7**: The dibromide **12** (50.8 mg, 31 μmol) and 4-aminophenylacetylene (19.0 mg, 0.162 mmol) were dissolved in a mixture of toluene (5 mL) and triethylamine (1 mL), and this solution was purged with argon. $[Pd(PPh_3)_2Cl_2]$ (8.0 mg) and CuI (9.0 mg) were added, and the resulting solution was heated at 50 °C for 1.5 h under argon. After the reaction mixture was filtered, the filtrate was purified by silica gel chromatography (eluent, CH_2Cl_2) to give **13** (56.0 mg, 30 μmol, 100%). ^{1}H NMR (500 MHz, $CDCl_3$): δ = 9.89 (d, J = 4.5 Hz, 4H; β-H), 9.07 (d, J = 5.0 Hz, 4H; β-H), 8.63 (d, J = 5.0 Hz, 4H; β-H), 8.09 (d, J = 1.5 Hz, 8H; Ar), 8.07 (d, J = 5.0 Hz, 4H; β-H), 7.75 (m, 4H; Ar), 7.72 (t, 4H; Ar), 7.38 (m, 4H; Ar), 1.47 (s, 72H; *t*Bu), H of NH_2 was not detected; MS (FAB): found 1728, calcd for $C_{112}H_{112}N_{10}Zn_2$, 1729.

The diamine **13** (37.4 mg, 21.6 μmol) and *N*-octyl-naphthalene-1,8-dicarboxyanhydride-4,5-dicarboxyimide (**14**) (20.0 mg, 0.0528 mmol) were dissolved in pyridine (5.0 mL), and the resulting solution was refluxed for 28 h under N_2. After the mixture was cooled, pyridine was removed by heating under reduced pressure. The crude mixture was purified by silica gel chromatography (eluent CH_2Cl_2) and preparative HPLC to give **7** (21.7 mg, 8.9 μmol, 41%). ^{1}H NMR (500 MHz, $CDCl_3$): δ = 9.93 (d, J = 5.0 Hz, 4H; β-H), 9.12 (d, J = 5.0 Hz, 4H; β-H), 8.87 (d, J = 7.5 Hz, 4H , NI), 8.74 (d, J = 7.5 Hz, 4H; NI), 8.67 (d, J = 5.0 Hz, 4H; β-H), 8.29 (d, J = 8.5 Hz, 4H; Ar), 8.11 (d, J = 5.0 Hz, 4H; β-H), 8.09 (d, J = 2.0 Hz, 8H; Ar), 7.73 (t, J = 2.0 Hz, 4H; Ar), 7.58 (d, J = 8.5 Hz, 4H , Ar), 4.13 (t, 4H; NI), 1.77 (m, 4H; NI), 1.53–1.28 (m, 20 + 72H; NI + *t*Bu), 0.88 (t, 6H; NI); MS (FAB): found 2449, calcd for $C_{156}H_{150}N_{12}O_8Zn_2$, 2447; UV/Vis (THF): λ_{max} (logε) = 440 (5.32), 476 (5.62), 583 (4.64), 637 (4.88) nm; fluorescence (THF): λ_{max} = 651 nm (λ_{max} = 580 nm).

5-(4-Trimethylsilylethynylphenyl)-15-pentafluorophenylporphyrin 15: 2,2′-Dipyrrylmethane (4.0 mmol) and 4-trimethylsilylethynylbenzaldehyde (2.0 mmol) and pentafluorobenzaldehyde (2.0 mmol) were dissolved in dry CH_2Cl_2 (600 mL). After addition of trifluoroacetic acid (4.05 mmol), the solution was stirred for 2.5 h at room temperature under N_2 in the dark. Then 2,3-dichloro-5,6-dicyano-1,4-benzoquinone (DDQ) (5.81 mmol) was added to the solution, and the stirring was continued for an additional 1 h. After addition of triethylamine (0.5 mL), the reaction mixture was passed through an alumina column with CH_2Cl_2 as eluent and the first porphyrin fraction was collected. Further purification was carried out by silica gel column chromatography (eluent; CH_2Cl_2/*n*-hexane) to give **15** (213 mg, 0.33 mmol, 17%). ^{1}H NMR (500 MHz, $CDCl_3$): δ 10.35 (s, 2H; *meso*), 9.47 (d, J = 4.5 Hz, 2H; β-H), 9.41 (d, J = 4.0 Hz, 2H; β-H), 9.06 (d, J = 4.5 Hz, 2H; β-H), 8.97 (d, J = 4.0 Hz, 2H; β-H), 8.97 (d, J = 8.5 Hz, 2H; Ar), 8.21 (d, J = 8.0 Hz, 2H; Ar), 0.40 (s, 9H; TMS), −3.15 (s, 2H; NH); MS (FAB): found 649, calcd for $C_{37}H_{25}F_5N_4Si$, 648; UV/Vis (THF): λ_{max} = 405, 499, 533, 574, 628 nm; fluorescence (THF): λ_{max} = 629, 693 nm (λ_{max} = 405 nm).

5-(4-Ethynylphenyl)-10-nitro-15-pentafluorophenylporphyrin 11: Zinc(II) 5-(4-trimethylsilylethynylphenyl)-15-pentafluorophenylporphyrin (0.170 mmol) and iodine (0.170 mmol) were dissolved in distilled $CHCl_3$. Then the reaction was started by addition of a solution of silver nitrite (0.230 mmol, 0.10 M acetonitrile solution). The mixture was stirred for 15 min at room temperature, and then poured into water, and extracted with $CHCl_3$. The organic layer was separated off, and washed with water, and sodium thiosulfate, and dried over anhydrous Na_2SO_4. Further purification was carried out by silica gel column chromatography (eluent; CH_2Cl_2/*n*-hexane) to give crude zinc(II) 5-(4-trimethylsilylethynylphenyl)-10-nitro-15-pentafluorophenylporphyrin. This product was dissolved in THF (10 mL), to which was added TBAF (0.30 mmol, 1 M THF solution).

© WILEY-VCH Verlag GmbH, D-69451 Weinheim, 2001
0947-6539/01/0714-3148 $ 17.50+.50/0 *Chem. Eur. J.* **2001**, *7*, No. 14

The mixture was stirred for 10 min at room temperature, and then passed through a short silica gel column with CH_2Cl_2 as a eluent. Further purification was carried out by silica gel column chromatography (eluent; CH_2Cl_2/*n*-hexane) to give zinc(II) 5-(4-ethynylphenyl)-10-nitro-15-pentafluorophenylporphyrin. This product was dissolved in CH_2Cl_2, and demetalation was carried out by treatment with 6N HCl. The organic layer was separated off, and washed with water and saturated $NaHCO_3$ aqueous solution, and dried over anhydrous Na_2SO_4 to give **11** (43 mg, 70 μmol, 41%). ^{1}H NMR (500 MHz, $CDCl_3$): $\delta = 10.38$ (s, 1H; *meso*), 9.45 (d, $J = 5.0$ Hz, 1H; β-H), 9.42 (d, $J = 5.0$ Hz, 1H; β-H), 9.39 (d, $J = 4.5$ Hz, 1H; β-H), 9.35 (d, $J = 4.5$ Hz, 1H; β-H), 9.05 (d, $J = 4.5$ Hz, 1H; β-H), 9.01 (d, $J = 5.0$ Hz, 1H; β-H), 8.97 (d, $J = 5.0$ Hz, 1H; β-H), 8.92 (d, $J = 5.0$ Hz, 1H; β-H), 8.19 (d, $J = 7.5$ Hz, 2H; Ar), 7.96 (d, $J = 8.0$ Hz, 2H; Ar), 3.37 (s, 1H; ethynyl), −3.04 (s, 2H; NH); MS (FAB): found 622, calcd for $C_{37}H_{16}F_5N_5O_2$, 621; UV/Vis (THF): λ_{max} (logε) = 413 (5.31), 508 (4.19), 582 (3.72), 637 (3.26) nm; fluorescence (THF): $\lambda_{max} = 643$, 703 nm ($\lambda_{ex} =$ 580 nm).

Tetramer 8: The dibromide **12** (22.1 mg, 3.3 μmol) and the ethynylated porphyrin **11** (13.0 mg, 20.9 μmol) were dissolved in a mixture of dry toluene (5 mL) and triethylamine (1 mL) and this solution was purged with argon. $[Pd_2(dba)_3]$ (4.4 mg) and Ph_3As (5.8 mg) were added, and the resulting solution was heated at 50 °C for 6 h under argon. After the reaction mixture was filtered, the filtrate was purified by silica gel chromatography (eluent CH_2Cl_2) and preparative HPLC (JAI-GEL, eluent $CHCl_3$). The fraction containing the target compound was collected and further purification was carried out by silica gel column chromatography (eluent; CH_2Cl_2/*n*-hexane) to give **8** (9.1 mg, 25%). ^{1}H NMR (500 MHz, $CDCl_3$): $\delta = 10.44$ (s, 2H; *meso*), 10.16 (d, $J = 4.5$ Hz, 4H; dimer-β-H), 9.49 (d, $J = 4.0$ Hz, 4H; FB-β-H), 9.46 (m, 4H; FB-β-H), 9.30 (d, $J = 4.0$ Hz, 2H; FB-β-H), 9.25 (d, $J = 4.5$ Hz, 2H; FB-β-H), 9.23 (d, $J = 4.0$ Hz, 4H; dimer-β-H), 9.01 (d, $J = 4.5$ Hz, 2H; FB-β-H), 8.96 (d, $J = 4.5$ Hz, 2H; FB-β-H), 8.73 (d, $J = 4.0$ Hz, 4H; dimer-β-H), 8.57 (d, $J = 7.5$ Hz, 4H; Ar), 8.48 (d, $J = 8.0$ Hz, 4H; Ar), 8.17 (m, 12H; dimer-β-H + Ar), 7.77 (m, 4H; Ar), 1.51 (s, 72H; *t*Bu), −2.92 (s, 4H; NH); MS (FAB): found 2737, calcd for $C_{164}H_{130}F_{10}N_{18}O_4Zn_2$, 2738; UV/Vis (THF): $\lambda_{max} = 415$, 475, 578, 640 nm; fluorescence (THF): $\lambda_{max} = 655$ nm (weak) ($\lambda_{max} = 580$ nm).

***meso,meso′*-Dibromo windmill porphyrin array 18**: The windmill porphyrin hexamer **16**[7b] (90.2 mg, 16.6 μmol) was dissolved in a mixture of $CHCl_3$ (90 mL) and pyridine (0.2 mL). NBS (33.8 μmol) was added to this solution and the solution was stirred for 10 min at room temperature. The mixture was poured into water and extracted with $CHCl_3$. The combined organic extract was washed with water and brine, and dried over Na_2SO_4. This crude product (**17**) was dissolved in a mixture of CH_2Cl_2, TFA, and 10% H_2SO_4, and the resulting solution was refluxed for 1 h. The mixture was poured into water, and extracted with CH_2Cl_2. The combined organic extract was successively washed with water, aqueous $NaHCO_3$ solution, and brine, and dried over Na_2SO_4. A saturated solution of Zn^{II} acetate in MeOH was added to the solution, and the resulting mixture was refluxed for 1 h, and poured into water. The porphyrin products were extracted with CH_2Cl_2. The combined organic extract was washed with water and brine, and dried over Na_2SO_4. Chromatography on a silica gel column (eluent CH_2Cl_2) gave **18** (87.9 mg, 15.7 μmol, 95%). ^{1}H NMR (500 MHz, $CDCl_3$): δ 10.30 (s, 4H; *meso*), 10.27 (d, $J = 4.0$ Hz, 4H; β-H), 10.12 (s, 4H; *meso*), 9.69 (d, $J = 4.0$ Hz, 4H; β-H), 9.30 (d, $J = 5.0$ Hz, 4H; β-H), 8.73 (d, $J =$ 8.0 Hz, 8H; Ar), 8.61 (d, $J = 5.0$ Hz, 4H; β-H), 8.49 (d, $J = 7.5$ Hz, 8H; Ar), 7.23 (m, 8H; Ar), 6.88 (s, 4H; Ar), 4.21 (br, 8H; hexyl), 4.06 (t + br, 16 + 8H; octyl + hexyl), 3.90 (br, 8H; hexyl), 3.83 (br, 8H; hexyl), 3.24 (s, 12H; Me), 2.85 (s, 12H; Me), 2.68 (s, 12H; Me), 2.63 (s, 12H; Me), 2.38–1.23 (m, 224H; hexyl + octyl), 1.03 (t, $J = 7.5$ Hz, 12H; hexyl), 0.95 (t, $J = 7.5$ Hz, 12H; hexyl), 0.83 (t, $J = 7.5$ Hz, 24H; octyl), 0.79 (t, $J = 7.5$ Hz, 12H; hexyl), 0.62 (t, $J = 7.5$ Hz, 12H; hexyl); MS (TOF): found 5561, calcd for $C_{344}H_{444}Br_2N_{24}O_8Zn_6$, 5596.

***meso,meso′*-Bisphenylethynylated windmill porphyrin array 2**: The dibromo windmill porphyrin hexamer **18** (22.0 mg, 3.9 μmol) and phenylacethylene (30 μmol) were dissolved in a mixture of toluene (5 mL) and triethylamine (1 mL), and this solution was purged with argon for 30 min. $[Pd(PPh_3)_2Cl_2]$ (12 mg) and CuI (9.0 mg) were added, and the resulting solution was heated at 50 °C for 5 h under argon. After the reaction mixture was filtered, the filtrate was separated by chromatography on a silica gel column (eluent CH_2Cl_2), and recylcing preparative HPLC (JAI-GEL, eluent $CHCl_3$) gave **2** (7.3 mg, 1.3 μmol, 33%). ^{1}H NMR (500 MHz, $CDCl_3$): $\delta = 10.37$ (d, $J = 4.5$ Hz, 4H; β-H), 10.31 (s, 4H; *meso*), 10.13 (s, 4H; *meso*), 9.72 (d, $J = 5.0$ Hz, 4H; β-H), 9.30 (d, $J = 4.5$ Hz, 4H; β-H), 8.75 (d, $J = 8.0$ Hz, 8H; Ar), 8.64 (d, $J = 4.5$ Hz, 4H; β-H), 8.50 (d, $J = 7.5$ Hz, 8H; Ar), 8.34 (d, $J = 7.0$ Hz, 4H; Ar), 7.78 (t, $J = 7.5$ Hz, 4H; Ar), 7.66 (m, 2H; Ar), 7.28 (s, 8H; Ar), 6.88 (s, 4H; Ar), 4.21 (br, 8H; hexyl), 4.06 (t + br, 16 + 8H; octyl + hexyl), 3.90 (br, 8H; hexyl), 3.83 (br, 8H; hexyl), 3.25 (s, 12H; Me), 2.85 (s, 12H; Me), 2.68 (s, 12H; Me), 2.63 (s, 12H; Me), 2.39–1.08 (m, 224H; hexyl + octyl), 1.00 (t, 12H; hexyl), 0.95 (t, $J = 7.5$ Hz, 12H; hexyl), 0.82 (t, $J = 7.5$ Hz, 24H; octyl), 0.78 (t, $J = 7.5$ Hz, 12H; hexyl), 0.61 (t, $J = 7.5$ Hz, 12H; hexyl); MS (TOF): found 5643, calcd for $C_{360}H_{454}N_{24}O_8Zn_6$,5638; UV/Vis (THF): λ_{max} (logε) = 415 (6.09), 442 (5.70), 476 (5.57), 545 (5.05), 580 (4.88), 635 (4.80) nm; fluorescence (THF): $\lambda_{max} = 659$ nm ($\lambda_{max} = 545$ nm).

***meso,meso′*-Bis(4-NI-linked phenyl)ethynylated windmill porphyrin array 3**: The dibromide **18** (55.3 mg, 9.92 μmol) and 4-aminophenylacetylene (7.3 mg, 62 μmol) were dissolved in a mixture of toluene (5 mL) and triethylamine (1 mL), and this solution was purged with argon for 30 min. $[Pd(PPh_3)_2Cl_2]$ (9 mg) and CuI (8 mg) were added and the resulting solution was heated at 50 °C for 7 h under argon. After the reaction mixture was filtered, the filtrate was separated by chromatography on a silica gel column (eluent CH_2Cl_2/*n*-hexane) to give 4-aminophenylethynyl porphyrin **19**. Without further purification, this crude product was used for the next reaction. The diamine **19** and the half-imide **14** (14.2 mg, 38 μmol) were dissolved in pyridine (5.0 mL), and the resulting solution was refluxed for 12 h under N_2. After the mixture was cooled, pyridine was removed by heating under reduced pressure. The crude mixture was purified by silica gel chromatography (eluent CH_2Cl_2) and HPLC(GPC-type, JAI-GEL, eluent $CHCl_3$) to give the NI-linked windmill porphyrin array **3** in a trace amount. The product eluted as a single band by HPLC (silica gel) as well as by size-exclusion GPC-HPLC. The ^{1}H NMR spectrum of **3** was rather broad and could not be analyzed. MS (TOF): found 6394, calcd for $C_{404}H_{494}N_{28}O_{16}Zn_6$, 6391; UV/Vis (THF): λ_{max} (logε) = 415 (6.07), 440 (5.68), 471 (5.54), 547 (5.02), 576 (4.86), 629 (4.81) nm; fluorescence (THF): $\lambda_{max} = 650$ nm ($\lambda_{max} = 545$ nm).

The porphyrin octameric model 4: The dibromide **18** (21.0 mg, 3.75 μmol) and the ethynylated porphyrin **11** (11.0 mg, 17.7 μmol) were dissolved in a mixture of dry toluene (5 mL) and triethylamine (1 mL), and this solution was purged with argon for 30 min. $[Pd_2(dba)_3]$ (6.0 mg) and Ph_3As (8.0 mg) were added, and the resulting solution was heated at 50 for 7 h under argon. After the reaction mixture was filtered, the filtrate was purified by silica gel chromatography (eluent CH_2Cl_2) and preparative HPLC (JAI-GEL, eluent $CHCl_3$). The fraction containing the target compound was collected and further purification was carried out by silica gel column chromatography (eluent; CH_2Cl_2) to give **4** (5.7 mg, 0.85 μmol, 23%). The product eluted as a single band by HPLC (silica gel) as well as by size-exclusion GPC-HPLC. The ^{1}H NMR spectrum of **4** was also too broadened for correct analysis. MS (TOF): found 6675, calcd for $C_{412}H_{474}F_{10}N_{34}O_{12}Zn_6$, 6677; UV/Vis (THF): $\lambda_{max} = 416$, 430 (sh), 472(sh), 547, 578, 637 nm; fluorescence (THF): $\lambda_{max} =$ 610, 630, 659 nm (weak) ($\lambda_{max} = 545$ nm).

***meso,meso′*-Bis(trimethylsilylethynyl)-substituted *meso*–*meso*-linked zinc(II) diporphyrin 20**: This compound was prepared from the dibrominated *meso*–*meso*-linked diporphyrin **12** and trimethylsilylacetylene by using $[Pd(PPh_3)_2Cl_2]$ and CuI; yield 53% (9.4 mg, 0.0056 mmol); ^{1}H NMR (500 MHz, $CDCl_3$): $\delta = 9.78$ (d, $J = 5.0$ Hz, 4H; β-H), 9.00 (d, $J = 4.0$ Hz, 4H; β-H), 8.57 (d, $J = 5.0$ Hz, 4H; β-H), 7.99 (m, 12H; β-H + Ar), 7.64 (s, 4H; Ar), 1.38 (s, 72H; *t*Bu), 0.58 (s, 18H; TMS); MS (FAB): found 1690, calcd for $C_{106}H_{118}N_8Si_2Zn_2$, 1691; UV/Vis (THF): λ_{max} (logε) = 435 (5.37), 468 (5.55), 579 (4.47), 627 (4.69) nm; fluorescence (THF): $\lambda_{max} = 648$ nm ($\lambda_{max} = 550$ nm).

***meso*-Phenylethynylated *meso*–*meso*-linked zinc(II) diporphyrin 21**: This compound was prepared from *meso*-monobrominated *meso*–*meso*-linked zinc(II) diporphyrin (4.5 μmmol) and phenylacethylene by using $[Pd(PPh_3)_2Cl_2]$ and CuI. Yield: 100% (7.2 mg, 4.5 μmmol). ^{1}H NMR (500 MHz, $CDCl_3$): $\delta = 10.38$ (s, 1H; *meso*), 9.95 (d, $J = 5.0$ Hz, 2H; β-H), 9.49 (d, $J = 4.5$ Hz, 2H; β-H), 9.18 (d, $J = 4.5$ Hz, 2H; β-H), 9.09 (d, $J =$ 4.5 Hz, 2H; β-H), 8.75 (d, $J = 5.0$ Hz, 2H; β-H), 8.62 (d, $J = 4.5$ Hz, 2H; β-H), 8.16 (d, $J = 5.0$ Hz, 2H; β-H), 8.10 (d, $J = 2.0$ Hz, 4H; Ar), 8.07 (d, $J =$ 2.0 Hz, 4H; Ar), 8.03 (d, $J = 5.0$ Hz, 2H; β-H), 7.71 (t, $J = 2.0$ Hz, 2H; Ar), 7.70 (t, $J = 2.0$ Hz, 2H; Ar), 7.61 (t, $J = 7.0$ Hz, 2H; Ar), 7.53 (d, $J = 7.0$ Hz, 2H; Ar), 7.34 (m, 1H; Ar), 1.46 (s, 36H; *t*Bu), 1.45 (s, 36H; *t*Bu); MS (FAB): found 1597, calcd for $C_{104}H_{106}N_8Zn_2$, 1598; UV/Vis (THF): λ_{max}

($\log\varepsilon$) = 435 (5.29), 465 (5.54), 554 (4.52), 579 (4.52), 629 (4.59) nm; fluorescence (THF): λ_{max} = 638 nm (λ_{ex} 580 nm).

The compounds **22** and **23** were prepared in a similar manner as for **20** and **21**.[7c]

Zinc(II) 5,15-bisphenylethynyl-10,20-bis(3,5-dictyloxyl)phenylporphyrin 22: ^{1}H NMR (500 MHz, $CDCl_3$): δ = 9.75 (d, J = 4.5 Hz, 4H; β-H), 9.06 (d, J = 4.0 Hz, 4H; β-H), 8.02 (d, J = 7.5 Hz, 4H; Ph), 7.57 (d, J = 7.5 Hz, 4H; Ph), 7.50 (t, J = 7.5 Hz, 2H; Ph), 7.36 (d, J = 1.5 Hz, 4H; Ar), 6.90 (t, J = 1.5 Hz,, 2H; Ar), 4.14 (t, J = 7.0 Hz, 8H; octyl), 1.88 (m, 8H; octyl), 1.51 (m, 8H; octyl), 1.35 – 1.28 (m, 32H; octyl), 0.86 (t, J = 7.0 Hz, 12H; octyl); MS (FAB): found 1237, calcd for $C_{80}H_{92}N_4O_4Zn$, 1237; UV/Vis (THF): λ_{max} ($\log\varepsilon$) = 449 (5.69), 595 (4.08), 649 nm (4.77); fluorescence (THF): λ_{max} = 654, 715 nm (λ_{ex} = 560 nm).

Zinc(II) 5-phenylethynyl-10,20-bis(3,5-dictyloxyl)phenylporphyrin 23: ^{1}H NMR (500 MHz, $CDCl_3$): δ = 10.19 (s, 1H; *meso*), 9.87 (d, J = 4.0 Hz, 2H; β-H), 9.33 (d, J = 5.0 Hz, 2H; β-H), 9.17 (d, J = 5.0 Hz, 2H; β-H), 9.14 (d, J = 5.0 Hz, 2H; β-H), 8.05 (d, J = 7.5 Hz, 2H; Ph), 7.58 (t, J = 7.0 Hz, 2H; Ph), 7.51 (d, J = 7.0 Hz, 1H; Ph), 7.39 (d, J = 2.0 Hz, 4H; Ar), 6.91 (t, J = 1.5 Hz, 2H; Ar), 4.15 (t, 8H; octyl), 1.88 (m, 8H; octyl), 1.50 (m, 8H; octyl), 1.39 – 1.27 (m, 32H; octyl), 0.86 (t, 12H; octyl); MS (FAB): found 1137, calcd for $C_{72}H_{88}N_4O_4Zn$, 1137; UV/Vis (THF): λ_{max} ($\log\varepsilon$) = 436 (5.75), 566 (4.34), 611 (4.42) nm; fluorescence (THF): λ_{max} = 614, 669 nm (λ_{ex} = 565 nm).

Acknowledgement

This work was supported by Grant-in-Aids for Scientific Research (No. 11223205 and No. 12440196) from the Ministry of Education,Science,Sports and Culture of Japan.

[1] a) R. J. Cogdell, J. P. Dekker, T. Gillbro, V. Sundström, *Biochim. Biophys. Acta* **1994**, *1187*, 1; b) T. Pullerits, V. Sundström, *Acc. Chem. Res.* **1996**, *29*, 381; c) V. Sundström, T. Pullerits, R. van Grondelle, *J. Phys. Chem.* **1999**, *103*, 2327.

[2] a) C. Kirmaier, D. Holten, *Photosynth. Res.* **1987**, *13*, 225; b) N. W. Woodbury, J. P. Allen in *Anoxugenic Photosynthetic Bacteria* (Eds.: R. E. Blankenship, M. T. Madigan, C. E. Bauer), Kluwer, Dordecht, **1994**, p. 527, and references therein.

[3] a) M. R. Wasielewski, *Chem. Rev.* **1992**, *92*, 435; b) D. Gust, T. A. Moore, A. L. Moore, *Acc. Chem. Res.* **1993**, *26*, 198; c) H. Kurreck, M. Huber, *Angew. Chem.* **1995**, *107*, 929; *Angew. Chem. Int. Ed. Engl.* **1995**, 34, 849; d) A. Osuka, N. Mataga, T. Okada, *Pure Appl. Chem.* **1997**, *69*, 797.

[4] a) G. Steinberg-Yfrach, P. A. Liddell, S.-C. Hung, A. L. Moore, D. Gust, T. A. Moore, *Nature* **1997**, *385*, 239; b) G. Steinberg-Yfrach, J.-L. Rigaud, E. N. Durantini, A. L. Moore, D. Gust, T. A. Moore, *Nature* **1998**, *392*, 479; c) A. Osuka, S. Nakajima, K. Maruyama, N. Mataga, T. Asahi, I. Yamazaki, Y. Nishimura, T. Ohno, K. Nozaki, *J. Am. Chem. Soc.* **1993**, *115*, 4577; d) A. Osuka, S. Nakajima, T. Okada, S. Taniguchi, K. Nozaki, T. Ohno, I. Yamazaki, Y. Nishimura, N. Mataga, *Angew. Chem.* **1996**, *108*, 98; *Angew. Chem. Int. Ed. Engl.* **1996**, *35*, 92; e) A. Osuka, S. Marumo, N. Mataga, S. Taniguchi, T. Okada, I. Yamazaki, Y. Nishimura, T. Ohno, K. Nozaki, *J. Am. Chem. Soc.* **1996**, *118*, 155.

[5] a) R. E. Martin, F. Diederich, *Angew. Chem.* **1999**, *111*, 1440; *Angew. Chem. Int. Ed.* **1999**, *38*, 1350; b) P. F. H. Schwab, M. D. Levin, J. Michl, *Chem. Rev.* **1999**, *99*, 1863; c) M. G. Vicente, L. Jaquinod, K. M. Smith, *Chem. Commun.* **1999**, 1771.

[6] D. Kuciauskas, P. A. Liddell, S. Lin, T. E. Johnson, S. J. Weghorn, J. S. Lindsey, A. L. Moore, T. A. Moore, D. Gust, *J. Am. Chem. Soc.* **1999**, *121*, 8604.

[7] a) A. Nakano, A. Osuka, I. Yamazaki, T. Yamazaki, Y. Nishimura, *Angew. Chem.* **1998**, *110*, 3172; *Angew. Chem. Int. Ed.* **1998**, *37*, 3023; b) A. Nakano, T. Yamazaki, Y. Nishimura, I. Yamazaki, A. Osuka, *Chem. Eur. J.* **2000**, *6*, 3254.

[8] a) A. Nakano, H. Shimidzu, A. Osuka, *Tetrahedron Lett.* **1998**, *39*, 9489; b) A. Nakano, Y. Yasuda, T. Yamazaki, S. Akimoto, I. Yamazaki, H. Miyasaka, A. Itaya, M. Murakami, A. Osuka, *J. Phys. Chem.* in press.

[9] a) D. P. Arnold, A. W. Johnson, M. Mahendran, *J. Chem. Soc., Perkin 1*, **1978**, 366 – 370; b) D. P. Arnold, L. J. Nitschinsk, *Tetrahedron* **1992**, *48*, 8781 – 8792; c) D. P. Arnold, D. A. James, *J. Org. Chem.* **1997**, *62*, 3460; d) D. P. Arnod, G. A. Heath, D. A. James, *J. Por. Phthal.* **1999**, *3*, 5.

[10] a) V. S.-Y. Lin, S. G. DiMagno, M. J. Therien, *Science*, **1994**, *264*, 1105; b) V. S.-Y. Lin, M. J. Therien, *Chem. Eur. J.* **1995**, *1*, 645; c) R. Kumble, S. Palese, V. S.-Y. Lin, M. J. Therien, R. M. Hochstrasser, *J. Am. Chem. Soc.* **1998**, *120*, 11489.

[11] a) H. L. Anderson, *Tetrahedron Lett.* **1992**, *33*, 1101; b) H. L. Anderson, *Inorg. Chem.*, **1994**, *33*, 972; c) P. L. Taylor, A. P. Wylie, J. Huuskonen, H. L. Anderson, *Angew. Chem.* **1998**, *110*, 1033; *Angew. Chem. Int. Ed.* **1998**, *37*, 986; d) P. N. Taylor, J. Huuskonen, G. Rumbles, R. T. Aplin, E. Williams, H. L. Anderson, *Chem. Commun.* **1998**, 909; e) H. L. Anderson, *Chem. Commun.* **1999**, 2323.

[12] a) L. R. Milgrom, G. Yahioglu, *Tetrahedron Lett.* **1995**, *36*, 9061; b) L. R. Milgrom, G. Yahioglu, *Tetrahedron Lett.* **1996**, *37*, 4069; c) L. R. Milgrom, R. Rees, G. Yahioglu, *Tetrahedron Lett.* **1997**, *38*, 4905.

[13] A. Osuka, H. Shimidzu, *Angew. Chem.* **1997**, *109*, 93; *Angew. Chem. Int. Ed. Engl.* **1997**, *36*, 135.

[14] A. Osuka, R.-P. Zhang, K. Maruyama, N. Mataga, Y. Tanaka, T. Okada, *Chem. Phys. Lett.* **1993**, *215*, 179.

[15] A. Osuka, G. Noya, S. Taniguchi, T. Okada, Y. Nishimura, I. Yamazaki, N. Mataga, *Chem. Eur. J.* **2000**, *6*, 33.

[16] S. G. DiMagno, S.-Y. Lin, M. Therien, J. *J. Org. Chem.* **1993**, *58*, 5983.

[17] S. Takahashi, Y. Kuroyama, K. Sonogashira, N. Hagihara, *Synthesis* **1980**, 627.

[18] O. Mongin, A. Gossauer, *Tetrahedron* **1997**, *53*, 6835 – 6846.

[19] a) M. P. Debreczeny, W. A. Svec, M. R. Wasielewski, *New J. Chem.* **1996**, *20*, 815; b) G. P. Wiederrecht, M. P. Niemczyk, W. A. Svec, W. R. Wasielewski, *J. Am. Chem. Soc.* **1996**, *118*, 81.

[20] P. G. Seybold. M. Gouterman, *J. Mol. Spectr.* **1969**, *31*, 1.

[21] A. Weller, *Z. Phys. Chem.* (Wiesbaden) **1982**, *93*, 1982.

[22] a) I. Yamazaki, N. Tamai, H. Kume, H. Tsuchiya, K. Oba, *Rev. Sci. Instrum.* **1985**, *56*, 1187; b) T. Yamazaki, I. Yamazaki, A. Osuka, *J. Phys. Chem. B* **1998**, *102*, 7858.

[23] S. Akimoto,T. Yamazaki, I. Yamazaki, A. Osuka, *Chem. Phys. Lett.* **1999**, *309*, 177.

[24] H. Miyasaka, T. Moriyama, A. Itaya, *J. Phys. Chem.* **1996**, *100*, 12609.

[25] A. Osuka, R.-P. Zhang, K. Maruyama, T. Ohno, K. Nozaki, *Bull. Chem. Soc. Jpn.* **1993**, *66*, 3773.

[26] a) N. Aratani, A. Osuka, Y. H. Kim, D. H. Jeoung, D. Kim, *Angew. Chem.* **2000**, *112*, 1517; *Angew. Chem. Int. Ed.* **2000**, *39*, 1458; b) H. S. Cho, N. W. Song, Y. H. Kim, S. C. Jeoung, S. Hahn, D. Kim, S. K. Kim, N. Yoshida, A. Osuka, *J. Phys. Chem. A* **2000**, *104*, 3287; c) Y. H. Kim, D. H. Jeong, D. Kim, S. C. Jeoung, H. S. Cho, S. K. Kim, N. Aratani, A. Osuka, *J. Am. Chem. Soc.* **2001**, *123*, 76.

[27] a) M. Kasha, *Radiat. Res.* **1963**, *20*, 55; b) M. Kasha, H. R. Rawls, M. A. El-Bayoumi, *Pure Appl. Chem.* **1965**, *11*, 371.

[28] a) A. Osuka, K. Maruyama, *J. Am. Chem. Soc.* **1988**, *110*, 4454; b) J. L. Sessler, M. R. Johnson, T.-Y. Lin, *Tetrahedron* **1989**, *45*, 4767.

[29] J. Rodriguez, C. Kirmaier, D. Holten, *J. Am. Chem. Soc.* **1989**, *111*, 6500.

[30] N. Yoshida, A. Osuka, *Tetrahedron Lett.* **2000**, *41*, 9287.

[31] T. Förster, *Discuss. Faraday Soc.* **1959**, *27*, 7.

[32] D. L. Dexter, *J. Chem. Phys.* **1953**, *21*, 836.

[33] N. Mataga, Y. Shibata, H. Chosrowjan, N. Yoshida, A. Osuka, *J. Phys. Chem. B* **2000**, *104*, 4001.

[34] a) D. Gust, T. A. Moore, A. L. Moore, C. Devadoss, P. A. Liddell, R. Hermant, R. A. Nieman, L. J. Demanche, J. M. DeGraziano, I. Gouni, *J. Am. Chem. Soc.* **1992**, *114*, 3590; b) M. P. Debreczeny, M. R. Wasielewski, S. Shinoda, A. Osuka, *J. Am. Chem. Soc.* **1997**, *119*, 6407; c) B. P. Krueger, G. D. Scholes, R. Jimenez, G. R. Fleming, *J. Phys. Chem. B* **1998**, *102*, 2284.

[35] a) G. G. Guzadyan, T.-H. Tran-Thi, T. Gustavsson, *J. Chem. Phys.* **1998**, *108*, 385; b) D. LeGourriérec, M. Andersson, J. Davidsson, E. Mukhtar, L. Sun, L. Hammarström, *J. Phys. Chem. A* **1999**, *103*, 557; c) M. Andersson, J. Davidsson, J. Hammarström, Korppi-Tommola, T. Peltola, *J. Phys. Chem. B* **1999**, *103*, 3258.

 © WILEY-VCH Verlag GmbH, D-69451 Weinheim, 2001 0947-6539/01/0714-3150 $ 17.50+.50/0

[36] A. Harriman, M, Hissler, O. Trompette, R. Ziessel, *J. Am. Chem. Soc.* **1999**, *121*, 2516.
[37] a) R. A. Marcus, *J. Phys. Chem.* **1956**, *24*, 966 and 979; b) R. A. Marcus, N. Sutin, *Biochim. Biophys. Acta* **1985**, *811*, 265.
[38] a) N. Mataga, *Adv. Chem. Ser.* **1991**, *228*, 91; b) T. Kakitani, A. Yoshimori, N. Mataga, *Adv. Chem. Ser.* **1991**, *228*, 45; c) N. Mataga, *Pure Appl. Chem.* **1993**, *65*, 1605; d) N. Mataga, H. Miyasaka, *Prog. React. Kinet.* **1994**, *19*, 317; e) T. Kakitani, N. Matsuda, A. Yoshimori, N. Mataga, *Prog. React. Kinet.* **1995**, *20*, 347; f) N. Mataga, *Pure Appl. Chem.* **1997**, *69*, 729; g) N. Mataga, H. Miyasaka, *Adv. Chem. Phys.* **1998**, *107*, 431.
[39] a) T. Ohno, A. Yoshimura, N. Mataga, *J. Phys. Chem.* **1986**, *90*, 3295; b) N. Mataga, Y. Kanda, T. Okada, *J. Phys. Chem.* **1986**, *90*, 3880; c) T. Ohno, A. Yoshimura, N. Mataga, S. Tazuke, Y. Kawanishi, *J. Phys. Chem.* **1989**, *93*, 3546; d) N. Mataga, T. Asahi, Y. Kanda, T. Okada, T. Kakitani, *Chem. Phys.* **1988**, *127*, 249.
[40] I. R. Gould, S. Farid, *Acc. Chem. Res.* **1996**, *29*, 522.
[41] a) T. Asahi, N. Mataga, *J. Phys. Chem.* **1989**, *93*, 6575; b) T. Asahi, N. Mataga, Y. Takahashi, T. Miyashi, *Chem. Phys. Lett.* **1990**, *171*, 309; c) T. Asahi, N. Mataga, *J. Phys. Chem.* **1991**, *95*, 1956; d) T. Asahi, M. Ohkohchi, M. Nataga, *J. Phys. Chem.* **1993**, *97*, 13132; e) H. Miyasaka, S. Kotani, A. Itaya, G. Schweitzer, F. C. De Schryver, N. Mataga, *J. Phys. Chem.* **1997**, *101*, 7978.
[42] a) D. Rehm, A. Weller, *Isr. J. Chem.* **1970**, *7*, 259; b) N. Mataga, Y. Kanda, T. Asahi, H. Miyasaka, T. Okada, T. Kakitani, *Chem. Phys.* **1988**, *127*, 239; c) A. Yoshimori, T. Kakitani, Y. Enomoto, N. Mataga, *J. Phys. Chem.* **1989**, *93*, 8316; d) S. Nishikawa, T. Asahi, T. Okada, N. Mataga, T. Kakitani, *Chem. Phys. Lett.* **1991**, *185*, 237; e) T. Kakitani, A. Yoshimori, N. Mataga, *J. Phys. Chem.* **1992**, *96*, 5385; f) N. Matsuda, T. Kakitani, T. Denda, N. Mataga, *Chem. Phys.* **1995**, *190*, 83.
[43] a) A. Osuka, S. Marumo, K. Maruyama, N. Mataga, Y. Tanaka, S. Taniguchi, T. Okada, I. Yamazaki, and Y. Nishimura, *Bull. Chem. Soc. Jpn.* **1995**, *68*, 262; b) P. A. Liddell, D. Kuciauskas, J. Sumida, B. Nash, D. Nguyen, A. L. Moore, T. A. Moore, D. Gust, *J. Am. Chem. Soc.* **1997**, *119*, 1400; c) M. Fujitsuka, O. Ito, H. Imahori, H. Yamada, Y. Sakata, *Chem. Lett.* **1999**, 721.
[44] a) G. L. Gaines, III, M. P. O'Neil, W. A. Svec, M. P. Niemczyk, M. R. Wasielewski, *J. Am. Chem. Soc.* **1991**, *113*, 719; b) T. Asahi, M. Ohkohchi, R. Matsusaka, N. Mataga, R. P. Zhang, A. Osuka, K. Maruyama, *J. Am. Chem. Soc.* **1993**, *115*, 5665; c) H. Heitele, F. Pöllinger, T. Härberle, M. E. Michel-Beyerle, H. A. Staab, *J. Phys. Chem.* **1994**, *98*, 7402; d) T. Härberle, J. Hirsch, F. Pöllinger, H. Heitele, M. E. Michel-Beyerle, C. Anders, A. Döhling, C. Krieger, A. Ruckermann, H. A. Staab, *J. Phys. Chem.* **1996**, *100*, 18269.
[45] J. M. Degraziano, P. A. Liddell, L. Leggett, A. L. Moore, T. A. Moore, D. Gust, *J. Phys. Chem.* **1994**, *98*, 1758.

Received: January 16, 2001 [F3003]